Arabian Journal of Chemistry (2022) **15**, 104014

King Saud University

Arabian Journal of Chemistry

www.ksu.edu.sa
www.sciencedirect.com

ORIGINAL ARTICLE

Adsorption of tetracycline using $CuCoFe_2O_4$@Chitosan as a new and green magnetic nanohybrid adsorbent from aqueous solutions: Isotherm, kinetic and thermodynamic study

Alireza Nasiri [a], Saeed Rajabi [b,c], Atefeh Amiri [d], Melika Fattahizade [d], Omolbanin Hasani [d], Ali Lalehzari [d], Majid Hashemi [e,*]

[a] *Environmental Health Engineering Research Center, Kerman University of Medical Sciences, Kerman, Iran*
[b] *Department of Environmental Health Engineering, School of Health, Shiraz University of Medical Sciences, Shiraz, Iran*
[c] *Student Research Committee, Shiraz University of Medical Sciences, Shiraz, Iran*
[d] *Department of Environmental Health Engineering, Faculty of Public Health, Kerman University of Medical Sciences, Kerman, Iran*
[e] *Student Research Committee, Kerman University of Medical Sciences, Kerman, Iran*

Received 28 February 2022; accepted 24 May 2022
Available online 30 May 2022

KEYWORDS

Green synthesis;
Antibiotic;
Adsorption process;
Nano-adsorbent;
Chitosan

Abstract Utilizing a new microwave-assisted method, $CuCoFe_2O_4$@Chitosan (Ch) was synthesized as a very strong, magnetically separable nano-adsorbent. The magnetic nanohybrid adsorbent was characterized by FESEM (Field emission scanning electron microscopy), EDS (energy dispersive X-ray), Mapping & Linescan, BET (Brunauer-Emmett-Teller), FTIR (Fourier-transform infrared spectroscopy), XRD (X-ray diffraction analysis), TGA (Thermogravimetric analysis), and VSM (Vibrating Sample Magnetometer) techniques. Then, the adsorption process of Tetracycline (TC) was investigated. The highest percentage of pollutant adsorption on the synthetic and real samples was recorded at an initial concentration of 5 mg/L, pH 3.5, contact time of 20 min, the dose of 0.4 g/L, and temperature of 25 °C, 93.07 %, and 67%, respectively. The TC adsorption process via the synthesized magnetic nanocomposite was consistent with the Freundlich isotherm model (R^2 = 0.992) and *pseudo*-second-order kinetic (K_2 = 0.267). The outcomes of thermodynamic analyses, which included entropy changes (ΔS = 10.122 J/mol.k), enthalpy changes (ΔH = −1.975 kJ/mol), and the Gibbs negative free energy (ΔG = −4.992 kJ/mol), revealed that the adsorption pro-

* Corresponding author at: Majid Hashemi, Student Research Committee, Kerman University of Medical Sciences, Kerman, Iran.
E-mail address: ma.hashemi@kmu.ac.ir (M. Hashemi).

Peer review under responsibility of King Saud University.

Production and hosting by Elsevier

https://doi.org/10.1016/j.arabjc.2022.104014

cess was spontaneous, favorable, and exothermic. The good magnetic properties allow easy separation after the adsorption operation. Finally, the efficiency of the nano-adsorbent in the removal process was 82.16% after four adsorption–desorption cycles. Some advantages of this research are a fast and green method for synthesis of adsorbent, fast kinetic, and magnetic properties to easy separation.

1. Introduction

Water is one of the most important factors on the planet since it is required for the existence of all living organisms, food production, economic growth, and public welfare (Javid et al., 2019). In most situations, it will be difficult to replace it, and its contamination will bring plenty of issues (Mahdizadeh et al., 2020; Malakootian et al., 2020c). People's water needs, on the other hand, will not be satisfied properly owing to the geographical and temporal distribution of water on the ground. As a result, one of the most serious human issues is water scarcity and pollution (Golkarami and Kaviani Rad, 2017; Singh and Gupta, 2016; Abbasi et al., 2021).

There are two types of water pollutants: natural and man-made. Industrial, agricultural, and household wastewater are examples of man-made polluted water resources (Malakootian et al., 2018a; Malakootian et al., 2019a; Malakootian et al., 2020a). The most varied contaminants that pollute water resources are produced by industrial wastewater, the majority of which are hazardous and carcinogenic (Malakootian et al., 2020a; Nasiri et al., 2022). Pharmaceutical pollutants are a class of industrial pollutants that enter wastewater via the pharmaceutical industry, home effluents, and hospital effluents, and then make their way into the environment. There are many different types of medicinal substances (Aghdasinia et al., 2019; Singh et al., 2020; Mahdizadeh et al., 2020).

Antibiotics are a class of medicines that are now used to treat infectious illnesses in people and animals caused by bacteria. This class of medicines accounts for roughly 15% of the overall drug makeup (Nasiri et al., 2019; Khan et al., 2021). Antibiotic dosages used by people and animals are expected to reach the sewage system in the range of 50 to 90% through urine and feces (Malakootian et al., 2019e; Malakootian et al., 2019d). Antibiotics, due to their complicated structure, are not biodegradable and accumulate in the environment (Zhao et al., 2020b; Balarak et al., 2020; Khan et al., 2020).

Tetracycline (TC) is a type of antibiotic with the molecular formula $C_{22}H_{24}N_2O_8$, and it is the world's second most commonly used antibiotic due to advantages such as low cost, high antimicrobial activity, and high effectiveness in the treatment and control of infectious diseases when compared to other antibiotics (Maleky et al., 2022). This antibiotic is one of the most often used antibiotics in humans and is used to treat illnesses caused by gram-positive and gram-negative bacteria, mycoplasma, fungus (Chlamydia), rickettsia, and parasites. High tetracycline levels in the body can cause problems with tooth and bone growth, liver poisoning, nausea, lack of appetite, mouth and throat sores, headaches, dizziness, and allergies, among other things (Jang et al., 2018; Gopal et al., 2020a; Zhou et al., 2020; Dai et al., 2020).

Water treatment is used to remove contaminants from water, aid in environmental preservation, and recycle water to decrease the use of current water resources, protect resources from pollution and other harmful causes, and reduce expenses and water consumption in line with standards (Malakootian et al., 2020c; Nasiri et al., 2021a; Malakootian et al., 2019b; Amiri et al., 2022). Physical methods such as membrane filtration and reverse osmosis, biological methods such as aerobic decomposition and activated sludge process, and chemical methods such as coagulation and flocculation, ion exchange, and advanced oxidation are all used to treat water today (Zhang et al., 2019; Malakootian et al., 2019c; Seow et al., 2016; Naddafi et al., 2021; Khoshnamvand et al., 2019b). Each technique has disadvantages such as high prices, hazardous sludge generation, high power consumption, high maintenance, and operational costs, and limited efficiency (Malakootian et al., 2019b; Javid et al., 2019; Naddafi et al., 2018; Yaghmaeian et al., 2016; Khoshnamvand et al., 2019a). In contrast to the disadvantages noted for the other techniques, the adsorbent method has several advantages, including high efficiency, environmental friendliness, cheap, simple but effective operation, no secondary pollution, no need for special equipment, no sludge production, and the ability to regenerate the adsorbent (Xiong et al., 2018; Malakootian et al., 2020b; Malakootian et al., 2019d; Altintig et al., 2022).

The adsorption process is one of the water treatment methods that use adsorbents to remove pollutants from the aqueous media (Chavoshani et al., 2018; Fadaei et al., 2017). The properties of the adsorbent and the characteristics of the treated effluent have an impact on the adsorption process' performance (Hashemi et al., 2017; Jaafarzadeh et al., 2014; Arica et al., 2019). The adsorption method is now widely utilized in industrial operations to treat a wide range of wastewaters. This method is also used to treat materials that are difficult to remove from water or that have a low concentration in the effluent (Noori Shamsi et al., 2018; Mehdinejad et al., 2018; Mohammadi et al., 2019; Atesa et al., 2017).

Surface and biological categories of adsorbents are utilized in adsorption techniques. Activated carbon, single-walled and multi-walled carbon nanotubes, and graphene oxide are examples of surface adsorbents, but their application is limited due to their high cost and complex and time-consuming separation from the reaction media (Pourzamani et al., 2018; Pourzamani et al., 2017; Sadeghi et al., 2018; Arica et al., 2017). As a result, nanoparticles such as iron oxides are employed to overcome these constraints, which, unlike surface adsorbents, offer benefits such as cost-effectiveness, application at a wide pH range, heat resistance, and storage (Malakootiana et al., 2021). Easy to use, high absorption capacity and speed, magnetic field separation, and regeneration capabilities. Biosorbents, also known as magnetic nano-sorbents, are adsorbents that include iron oxide nanoparticles (Hashemzadeh et al., 2018; Fatehi et al., 2018; Bayramoglu and Arica, 2021).

Iron oxide nanoparticles are powerful adsorbents; however, their surface area is decreased owing to aggregation and cohesion, lowering their adsorption effectiveness. Because iron oxides contain a vast variety of metals that can produce distinct magnetic characteristics and crystal structures, they are separated into numerous classes (Malakootian et al., 2019g). Orthoferrite ($MFeO_3$), garnet ($M_3Fe_5O_{12}$), hexaferrite ($BaFe_{12}O_{19}$ and $SrFe_{12}O_{19}$), and ferrite spinels are the most prevalent categories of known iron oxides so far. Ferrite spinels have the chemical formula AB_2O_4, where A and B are metal cations in the tetrahedral and octahedral positions, respectively. Divalent cations such as Cu, Zn, Fe, Co, Ni, and Mn are the most frequent metal cations found in the structure of these iron oxides. Ferrite spinels, on the other hand, are the most extensively utilized ferrites because of their high magnetic strength, high thermal and chemical resistance, high surface area, and nanotechnology (Vinosha et al., 2021; Dutta et al., 2019; Malakootian et al., 2018a).

Cobalt ferrite and its derivatives are among the most commonly studied ferrite spinels, and this might be owing to the compound's great stability in a variety of reaction conditions, cost-effectiveness, simplicity of separation by an external magnetic field, and ability to

be reused for several cycles. On the other hand, Cobalt ferrite is a well-known strong magnetic compound with sturdy magneto-crystalline inhomogeneity, high coercivity, modest magnetization, high magnetostrictive coefficient, high hardness, electrical barrier properties, impressive chemical stability, mechanical rigidity, and high electrical resistance with low flux losses. There are several ways for modifying magnetic nano-sorbents, solving nano-sorbent problems, and maximizing magnetic adsorbent performance, including the use of organic ligands (like thiols), polymer bonding (like chitosan), and inorganic species (like silica) (Malakootian et al., 2018b; Kurian and Thankachan, 2021; SOUFI et al., 2021).

Chemically modified polysaccharides have been intensively researched in the hopes of developing novel biomaterials with unique physicochemical characteristics for removing contaminants from water and wastewater. To reduce treatment costs while minimizing the formation of hazardous by-products at the end of the process, eco-friendly adsorbents (polysaccharides) must be used (Crini, 2005). Due to the presence of functional groups such as hydroxyl, amino, or acetamido on their surface, polysaccharides offer distinctive features such as a unique structure, good chemical stability, strong reactivity, affinity, and selectivity for pollutants and aromatic compounds (Mittal et al., 2016).

Chitosan (Ch) is a polysaccharide produced by organisms and plants. Biodegradability, antibacterial activity, fungal growth inhibition, non-toxicity, low cost, and high-water solubility are all benefits of chitosan. Because of its OH and NH_2 functional groups, chitosan is employed as an adsorbent modifier in the adsorption process, preventing adsorption buildup and reducing competition for the adsorbent's active site, as well as increasing adsorption efficiency. Adsorbents containing chitosan offer several benefits, including reusability, lack of secondary contamination, and high adsorption capacity (Alizadeh et al., 2017; Wang and Zhuang, 2017).

Various magnetic sorbents, including CTM@Fe_3O_4 (Ahamad et al., 2020), MOF-chitosan (Zhao et al., 2020a), Fe_3O_4-chitosan (Asgari et al., 2020), $CoFe_2O_4$/graphene oxide (Chang et al., 2020), SiO_2@$CoFe_2O_4$/GO (Santhosh et al., 2017), $CoFe_2O_4$/AC (Qiu et al., 2016), $CoFe_2O_4$@vacancy@mSiO_2 (Lu et al., 2019), $CuFe_2O_4$/activated carbon (Zhang et al., 2011), $CoFe_2O_4$/Co_xFe_y/AC (Xu et al., 2014), Chitosan/SiO_2/Fe_3O_4/AC (Li et al., 2017), $CoFe_2O_4$-chitosan-graphene (Zhang et al., 2014), MWCNT/$CoFe_2O_4$–NH_2 (Zhou et al., 2014), $CoFe_2O_4$-TETA-GO (Sun et al., 2016) have been produced and employed in the adsorption process thus far.

In this work, $CuCoFe_2O_4$@Ch was synthesized for the first time in the presence of Ch biopolymer as a new magnetic nano-adsorbent for TC removal. The advantages of this magnetic nano-adsorbent include fast, green, and high-efficiency synthesis with microwave-assisted in the presence of Ch as a biopolymer, no use of toxic solvents, and surfactants. The presence of Ch during the preparation of $CuCoFe_2O_4$@Ch leads to a larger surface area of the magnetic nanocomposite. Also, amine and hydroxyl groups in Ch cause the electrostatic attraction between TC and the adsorbent surface. As a result, a larger number of TC molecules are placed on the $CuCoFe_2O_4$@Ch surface and trigger more interaction for improving the adsorption. Additionally, Adsorption isotherms, kinetics, and thermodynamics were examined while optimizing process parameters such as solution pH, initial concentration of TC, adsorbent dosage, and contact time. Reusability and chemical stability of nano-biocomposite were also assessed.

2. Materials and methods

2.1. Chemicals and instrumentation

Cobalt (II) chloride hexahydrate ($CoCl_2{\cdot}6H_2O$), iron (III) chloride hexahydrate ($FeCl_3{\cdot}6H_2O$), copper (II) chloride dihydrate ($CuCl_2{\cdot}2H_2O$), chitosan (Ch), sodium hydroxide (NaOH), and hydrogen chloride (HCl) were furnished by Sigma Aldrich and Merck companies, and the Tetracycline was purchased from Darou Pakhsh Pharmaceutical Manufacturing Company (Tehran, IRAN). Deionized water was used to make the experiment solutions. HCl and NaOH (1N) were used to alter the pH of the solutions, and the pH was measured using a pH meter (HANNA instruments, pH 212). A UV–vis spectrophotometer (SHIMADZU, UV-1800) was used to detect the concentration of TC at a maximum wavelength of 357 nm.

2.2. Preparation of $CuCoFe_2O_4$@Ch

As shown in Fig. 1, in the presence of chitosan polysaccharide, copper chloride, cobalt chloride, and iron chloride III salts were utilized to make magnetic nano-adsorbent. To begin, a specific stoichiometric ratio (0.5:0.5:2) of copper chloride (0.85 g), cobalt chloride (1.19 g), and iron chloride III (5.4 g) salts were dissolved in 100 mL of distilled water, respectively. Chitosan (1 g) was added to the reaction vessel after the chloride salts have been dissolved and agitated. The reaction media was subsequently alkalized using sodium hydroxide (6 gr), and the process was finished by irradiating the reaction vessel in the

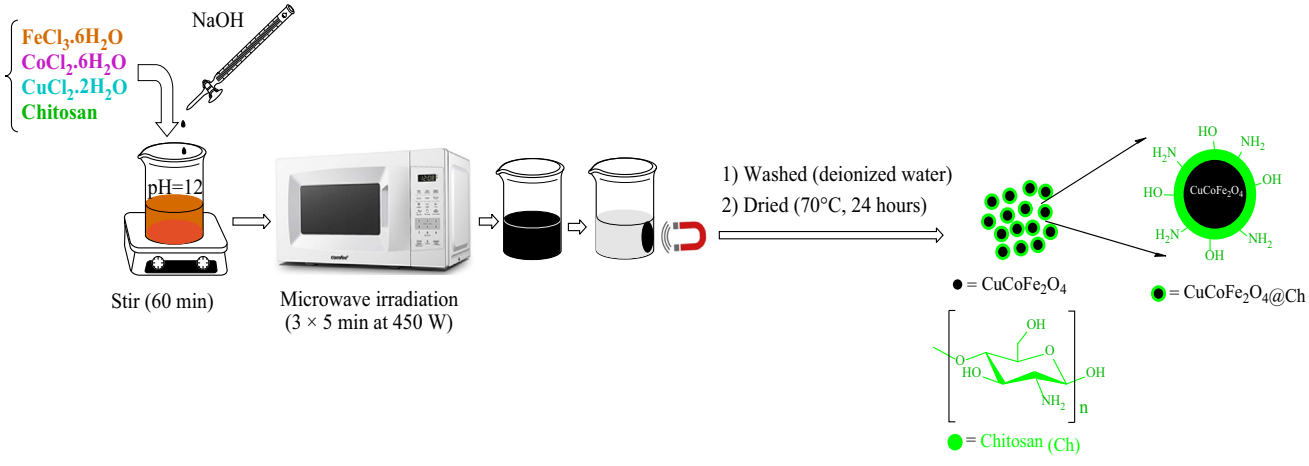

Fig. 1 Schematic of $CuCoFe_2O_4$@Ch synthesis.

microwave. A black copper-cobalt ferrite precipitate was formed. After removing the sediment and rinsing it with water, it was dried in it for 24 h at 70 °C in the oven (Rajabi et al., 2022; Nasiri et al., 2021a; Nasiri et al., 2019).

2.3. Instrument details

XRD, FESEM, EDS-Mapping and Line scan, FTIR, VSM, BET, and TGA techniques were used to study the structure of this black precipitate, which operates as a magnetic nano adsorbent. XRD to determine the magnetic nano-crystal adsorbent's structure and phase (PHILIPS PW1730), FESEM to investigate the structure, composition, and surface structure of magnetic nano-adsorbents on the nanoscale (TESCAN MIRA III), EDS-Mapping and Line scan to investigate the element weight percentages, types, and distributions at the surface of magnetic nano-adsorbent (TESCAN MIRA II, SAMX Detector), FTIR to investigate chemical bonding in magnetic nano-adsorbents and determine functional groupings (AVATAR, Thermo), VSM to determine the magnetic properties of magnetic nano-adsorbent (LBKFB, Kashan Kavir Magnet Company), BET to determine the size of a magnetic nano adsorbents specific region (BELSORP MINI II), and TGA to determine the thermal resistance of nanoparticles (SDT, Q600) techniques were used to study the structure of the resultant adsorbent. After confirming the magnetic nano adsorbent's physical and chemical structure, it was used to adsorb TC from an aqueous medium.

2.4. Batch adsorption experiments

pH, adsorbent dosage, initial tetracycline concentration, temperature, and contact time were all examined and adjusted as factors impacting the adsorption process. Antibiotic concentrations of 5, 10, 15, 20, and 30 mg/L were generated from stock tetracycline solution with 500 mg/L concentration. The values of 0.2, 0.4, 0.6, 0.8, and 1 g/L were investigated to optimize the adsorbent dosage. The researchers looked at pH ranges of three to eleven (3.5, 5.5, 7.5, 9.5, and 11.5), contact durations of 5, 10, 15, 20, 25, and 30 min, and temperatures of 25, 30, 35, and 40 degrees Celsius. The adsorption efficiency of tetracycline (Eq. (1)) and the adsorption capacity of the adsorbent (Eq. (2)) were determined using the formulae below:

$$Removal\ \ Efficiency(\%) = \frac{C_0\text{-}C_t}{C_0} \times 100 \quad (1)$$

$$Q = \frac{(C_0\text{-}C_t)V}{M} \quad (2)$$

C_0 and C_t (mg/L) indicate TC concentrations before and after contact time, respectively; Q represents adsorption capacity (mg/g), V represents sample volume (L), and M represents adsorbent dosage (g) (Tamaddon et al., 2020).

2.5. Determine of pH_{zpc}

Using 50 mL of KCl 0.1 M solution at six pHs (2, 4, 6, 8, 10, and 12) and 0.01 g of magnetic nanoparticles, the pH_{zpc} was measured. Then place ready solutions on the shaker after 24 h and measure the ultimate pH. The resultant curve was shown as X = starting pH and Y = ΔpH using the equation ΔpH = pH_{final}-$pH_{initial}$. The pH_{zpc} is the point on the X-axis where the curve crosses (Datta et al., 2017; Malakootian et al., 2018b).

3. Results and discussion

3.1. Characterization of the synthesized magnetic nano-adsorbent

3.1.1. FTIR

The KBr pellet was compared to the FTIR spectra of Ch and $CuCoFe_2O_4$@Ch, displayed in Fig. 2, to identify the functional group of the generated nanoparticles. The Ch vibration absorption bands were the following based on FTIR spectra: O—H stretching at 3418 cm^{-1}, C—H symmetric and asymmetric stretching at 2922 and 2862 cm^{-1}, NH primary amine bends at 1621 cm^{-1}, C—O in the primary alcoholic group at 1383 cm^{-1}, asymmetric stretching of the C—O—C bridge at 1155 cm^{-1}, C—O stretching at 1066 and 1028 cm^{-1}, and —NH_2 free amino group at 1025 cm^{-1}, and C—N stretching at 860 cm^{-1} (de Carvalho Oliveira et al., 2010; Oliveira et al., 2015; Rodrigues Filho et al., 2007; Sekiguchi et al., 2003; Wiercigroch et al., 2017; Fernandes Queiroz et al., 2015; Varma and Vasudevan, 2020).

Furthermore, the vibration absorption bands for $CuCoFe_2O_4$@Ch nano-adsorbent were the following based on FTIR spectra: O—H stretching at 3431 cm^{-1}, —CH_2 stretching at 2923 cm^{-1}, NH primary amine bends at 1633 cm^{-1}, C—O in the primary alcoholic group at 1383 cm^{-1}, and —NH_2 free amino group at 1069 cm^{-1} that the presence of chitosan in the nano-adsorbent structure is confirmed by these bands. Also, two confirming absorption peaks of the metal spinel ferrite structure were seen at 593 and 417 cm^{-1}, respectively, showing the metal cation at the octahedral site M_{octa}-O and the intrinsic stretching vibrations of the metal cation at the tetrahedral site M_{tetra}-O that were attributed to $CuCoFe_2O_4$@Ch's distinctive peak (El-Sayed, 2002; Mallapur et al., 2009; Waldron, 1955; Fernandes Queiroz et al., 2015; Varma and Vasudevan, 2020).

3.1.2. FESEM

The morphology, shape, and size of the $CuCoFe_2O_4$@Ch produced were determined using FESEM images. Fig. 3(a-c) show FESEM images of $CuCoFe_2O_4$@Ch generated in the presence of chitosan as a biopolymer. The inclusion of Ch in the $CuCoFe_2O_4$@Ch structure leads to the development of a smooth, pseudo spherical, and loosely aggregated magnetic nano-adsorbent. Fig. 3(d) depicts the particle size distribution. The average particle size of $CuCoFe_2O_4$@Ch is 25–30 nm, according to the particle size distribution histogram.

3.1.3. EDS, Mapping & Linescan

The purity and chemical structure of the $CuCoFe_2O_4$@Ch that had been generated were assessed using EDS analysis (Fig. 4). $CuCoFe_2O_4$@Ch magnetic nano-adsorbent includes 43.23% O, 25.51% Fe, 14.76% C, 7.28% Co, 4.87% Cu, and 4.34 % N, according to EDS results, which are all within the expected range.

Mapping is the study of how components are distributed at a high level of detail. It was used to investigate $CuCoFe_2O_4$@-

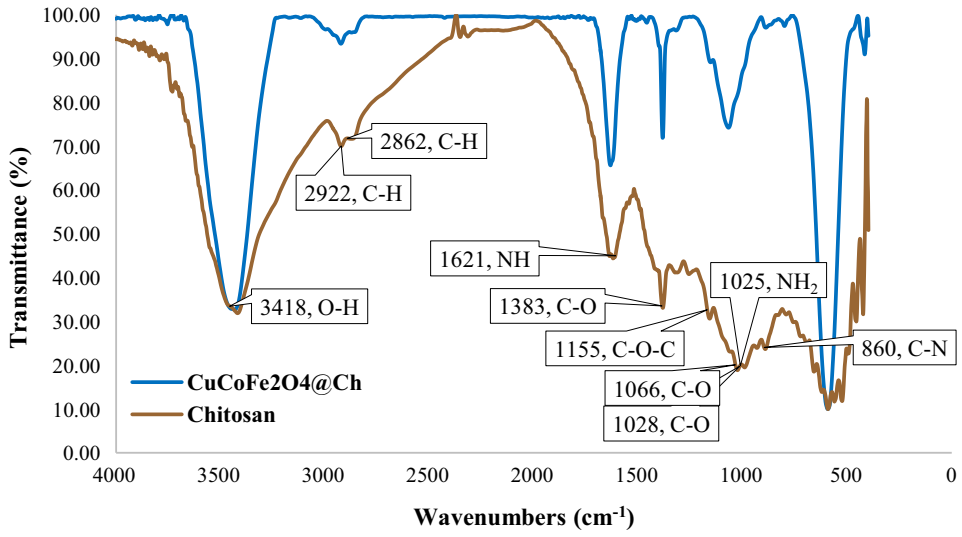

Fig. 2 FTIR of Chitosan and $CuCoFe_2O_4$@Ch magnetic nanocomposite.

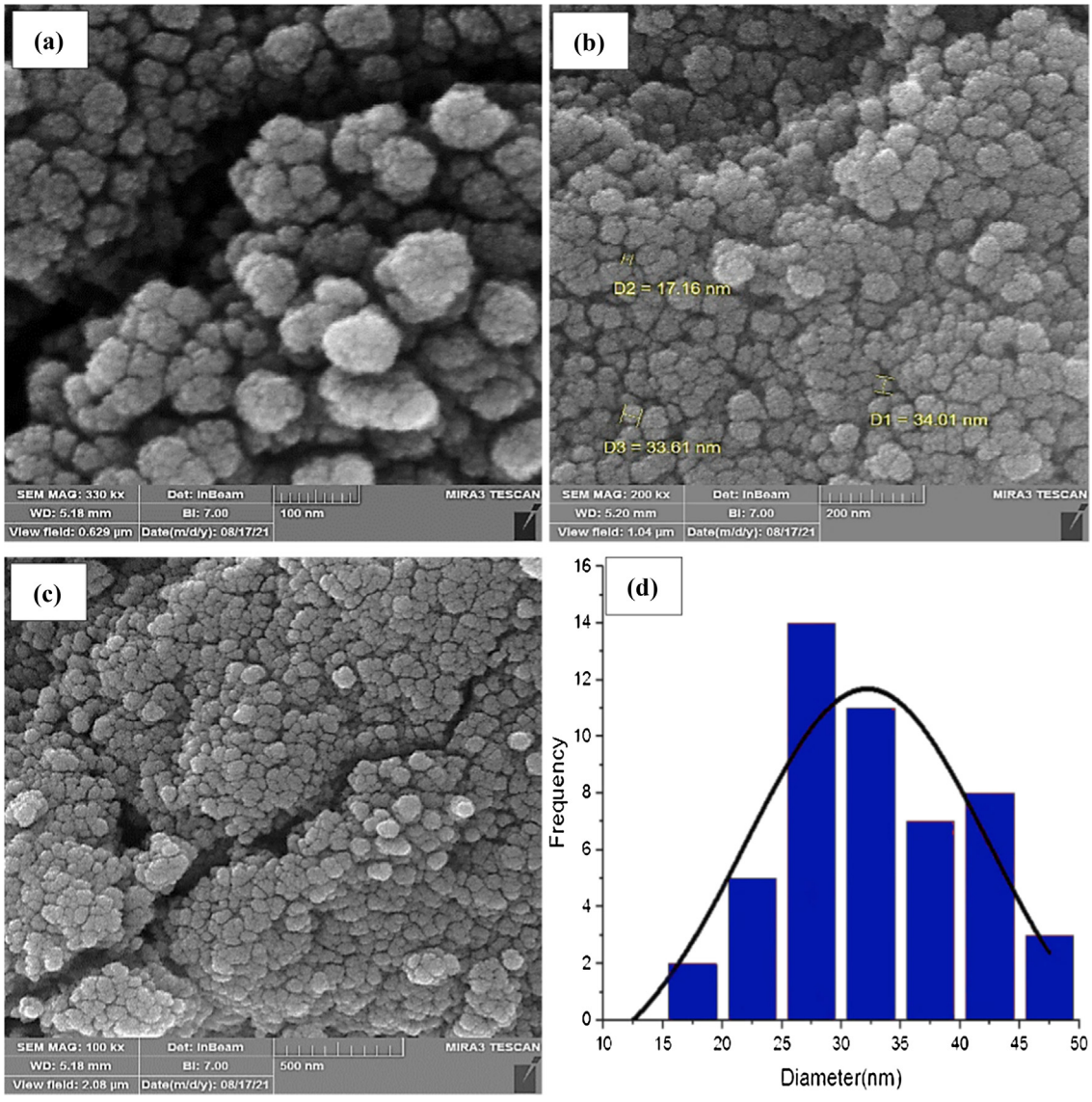

Fig. 3 FESEM images (a-c) and histogram of the particles size distribution (d) of $CuCoFe_2O_4$@Ch magnetic nanocomposite.

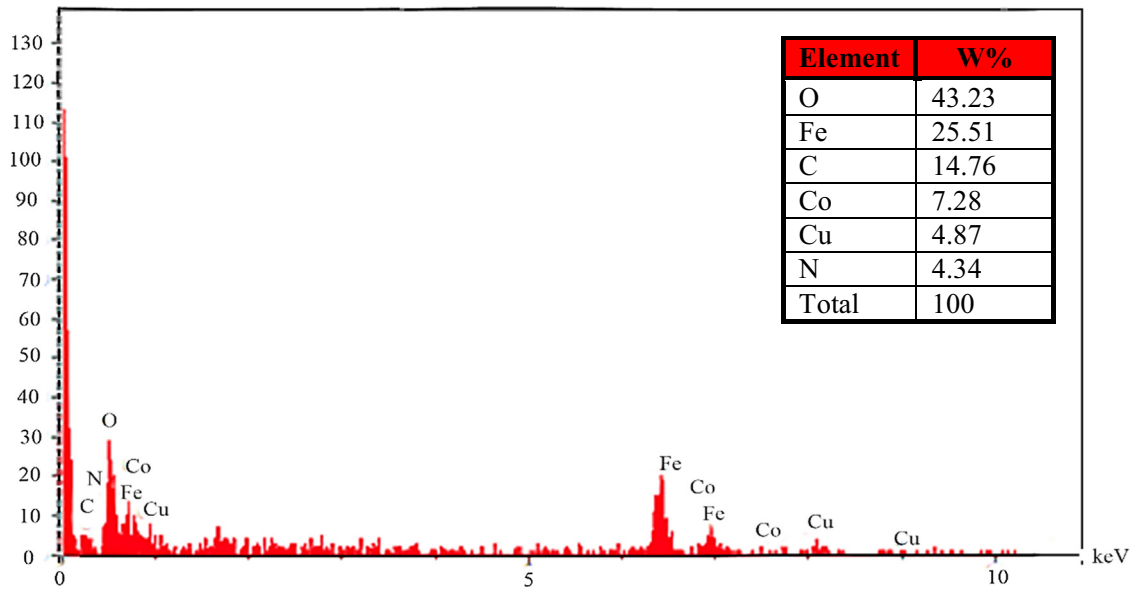

Fig. 4 EDS of $CuCoFe_2O_4$@Ch magnetic nanocomposite.

Ch element dispersion. Cu, Co, Fe, O, N, and C all showed a homogeneous distribution, suggesting that the synthesized $CuCoFe_2O_4$@Ch had a high uniformity, as shown in Fig. 5a. Furthermore, line scan analysis (Fig. 5b) is the investigation of element concentration changes across various regions of the $CuCoFe_2O_4$@Ch that allowed the Mapping analysis to be performed.

3.1.4. XRD

XRD analysis was used to investigate the structure, phases, and crystalline content of $CuCoFe_2O_4$@Ch. The total results are shown in Fig. 6. According to the Joint Committee on Powder Diffraction Standards (JCPDS 96-591-0064), the $CuCoFe_2O_4$@Ch crystal phase structure and XRD pattern with diffraction peaks at $2\theta \approx 30.32°$, 35.75°, 43.37°, 53.97°, 57.27°, 62.90°, and 74.40° are indexed to the cubic spinel phase of $CuCoFe_2O_4$ (Malakootian et al., 2018b) and $2\theta \approx 18.34°$ with a weak peak associated with chitosan structure (Liu et al., 2021). There in the ultimate nano-adsorbent structure, the intensity of the chitosan peak has been decreased but not obliterated. Because of its involvement in the reaction during adsorbent production, chitosan's peak intensity has been reduced. According to the findings, the $CuCoFe_2O_4$ crystal structure was successfully preserved in the composition containing Ch. The average crystallite size of $CuCoFe_2O_4$@Ch was calculated and it was 10.56 nm.

3.1.5. BET

Fig. 7 depicts the $CuCoFe_2O_4$@Ch adsorption/desorption isotherm, BET-BJH specific surface area, and t-plot (Fig. 7a-d). The N_2 adsorption/desorption experiments were used to examine the BET surface area of $CuCoFe_2O_4$@Ch nanocomposite. The BET equation was used to compute the monolayer volume of adsorbed gas, which can then be used to calculate the surface area of the adsorbent (Malakootian et al., 2018b). Using the BET plot, the specific surface area, mean pore diameter, and total pore volume ($p/p_0 = 0.990$) of synthesized magnetic nano-adsorbent were determined to be 79.057 m^2/g, 8.704 nm, and 0.172 cm^3/g, respectively. The intensity of the contact between the sample surface and the adsorptive surface, as well as the presence or lack of pores, are used to classify adsorption isotherms. The International Union of Pure and Applied Chemistry (IUPAC) classifies pores as microporous, mesoporous, or macroporous. A mesoporous material, according to the IUPAC, has pores ranging in size from 2 to 50 nm. Microporous pores have a diameter of fewer than 2 nm, and macroporous pores have a diameter of more than 50 nm. The figure shows a Type-IV isotherm with a prominent hysteresis loop between both the adsorption and desorption branches, showing that is $CuCoFe_2O_4$@Ch, a mesoporous material (Ariga et al., 2012).

3.1.6. VSM

As shown in Fig. 8, Saturation magnetization (Ms), residual magnetization (Mr), and coercive force (Hc) values for $CuCoFe_2O_4$@Ch were 17.49 emu/g, 7.02 emu/g, and 50 Oe, respectively. These findings show that $CuCoFe_2O_4$@Ch has high magnetic strength. The strong magnetic property of the $CuCoFe_2O_4$@Ch magnetic nano-adsorbent assists considerably in the separation of the adsorbent from the reaction medium during the recovery and reuse phases, and it can be separated quickly using an external magnet.

3.1.7. TGA

To show the importance of adsorbent thermal stability in industrial applications, a TGA of $CuCoFe_2O_4$@Ch was performed in an N_2 environment with a temperature range of ambient temperature to 600 °C (20 °C min^{-1}). The thermal deterioration of $CuCoFe_2O_4$@Ch occurred in three stages (Fig. 9). The first step of mass loss is attributed to adsorbed water loss in the temperature range of 20–100 °C. The major decomposition of Ch, which begins at 100 °C and reaches a maximum rate of 410 °C, is the second stage. The 18% mass loss in this stage is due to polysaccharide chain breakage,

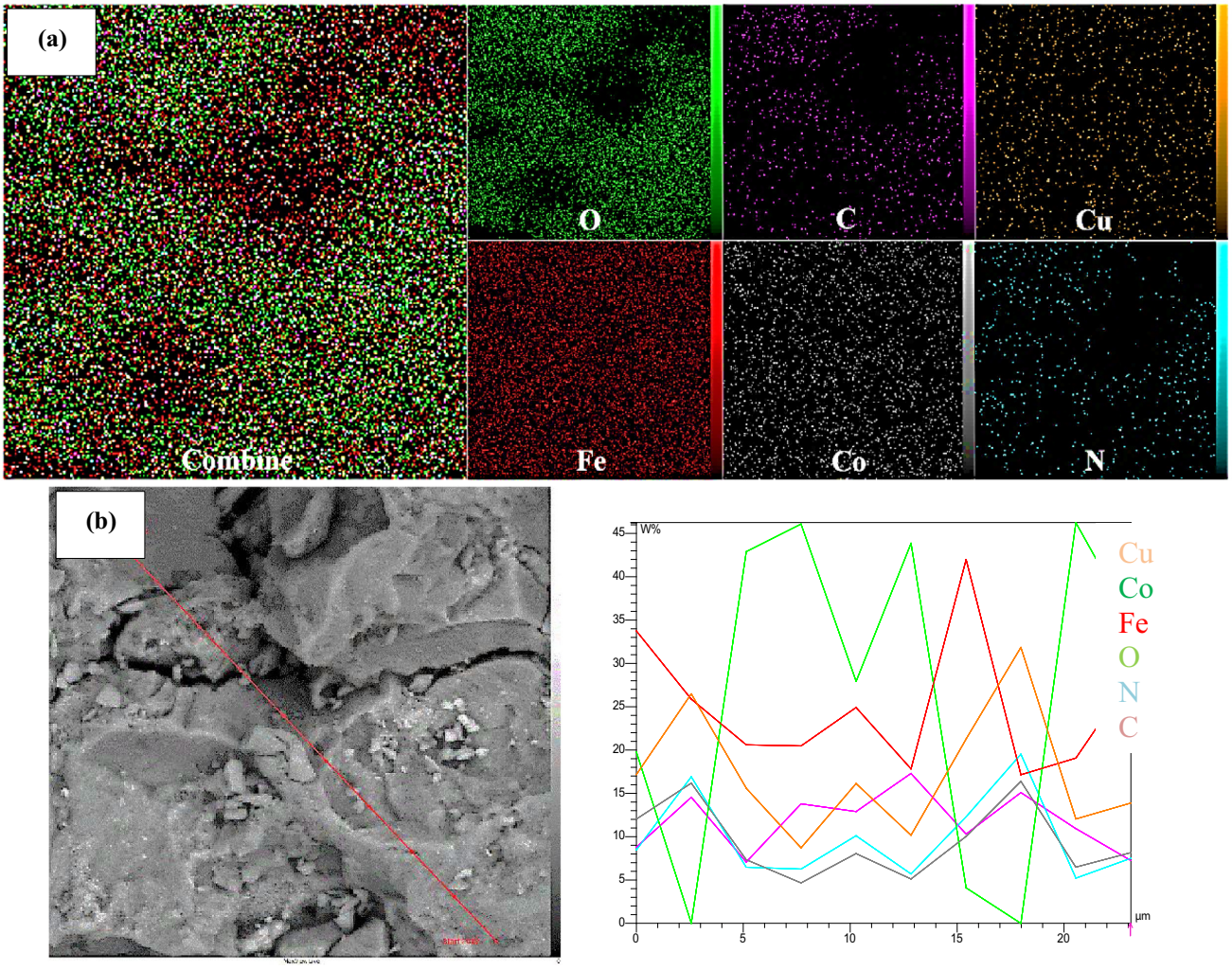

Fig. 5 Mapping (a), and Line scan (b) of $CuCoFe_2O_4$@Ch magnetic nanocomposite.

vaporization, and removal of breakdown products (including dehydration, deamination, deacetylation, breaking of glycoside bonds, and pyranose ring-opening) (Ziegler-Borowska et al., 2015). There was no substantial weight reduction in the third phase, which lasted from 410 to 600 °C. According to the data, the adsorbent lost 21.13% (1.096 mg) of its weight at 600 °C. The $CuCoFe_2O_4$@Ch is thermally stable, according to this finding.

3.2. The impact of effective parameters on the adsorption

3.2.1. Effect of adsorbent dose on TC adsorption

Adsorbent dosages of 0.2, 0.4, 0.6, 0.8, and 1 g/L were investigated in vitro at a temperature of 25 °C, pH 4, and a TC initial concentration of 5 mg/L in this work. As shown in Fig. 10, with increasing the adsorbent dose from 0.2 to 1 g/L, the removal efficiency of TC increased from 84.2 to 97.4%. As the efficiency of removal of TC has risen, but efficiency gains were raised between 0.2 and 0.4 g/L, from 84.2 to 91.2%, and from 0.4 to 0.6 g/L, the efficiency gains of removal of TC were around 1%. It is really low and insignificant. As a consequence, the absorbent dosage that worked best for this procedure was 0.4 g/L. The explanation for the increased TC removal efficiency with increasing the adsorbent dosage might be because the active sites and contact surface of the adsorbent with TC increase with increasing the adsorbent dose. Furthermore, even though the quantity of nano-sorbent is increased, since some TC is adsorbed on the adsorbent, the concentration of TC in the reaction media is substantially reduced, and as a response, the TC contact with the nano-sorbent diminishes. As a consequence, the removal efficiency of TC improves very slightly (Aslan et al., 2016; Nasiri et al., 2021b). However, due to the constant concentration and volume of TC solution, increasing the adsorbent dose causes the active adsorbent sites to remain unsaturated, and also with increasing the adsorbent dose, the accumulation of adsorbent in the aqueous solution increases, and the actual adsorption capacity of the adsorbent is reduced, lowering the TC removal efficiency (Takdastan et al., 2016). Guo et al., In a study of tetracycline adsorption, concluded that increasing the adsorbent dose increases the adsorption efficiency of tetracycline, but after reaching the best adsorbent dose, the subsequent dose increase has little effect on efficiency. The results of this study are very similar to the results of the present study (Guo et al., 2017).

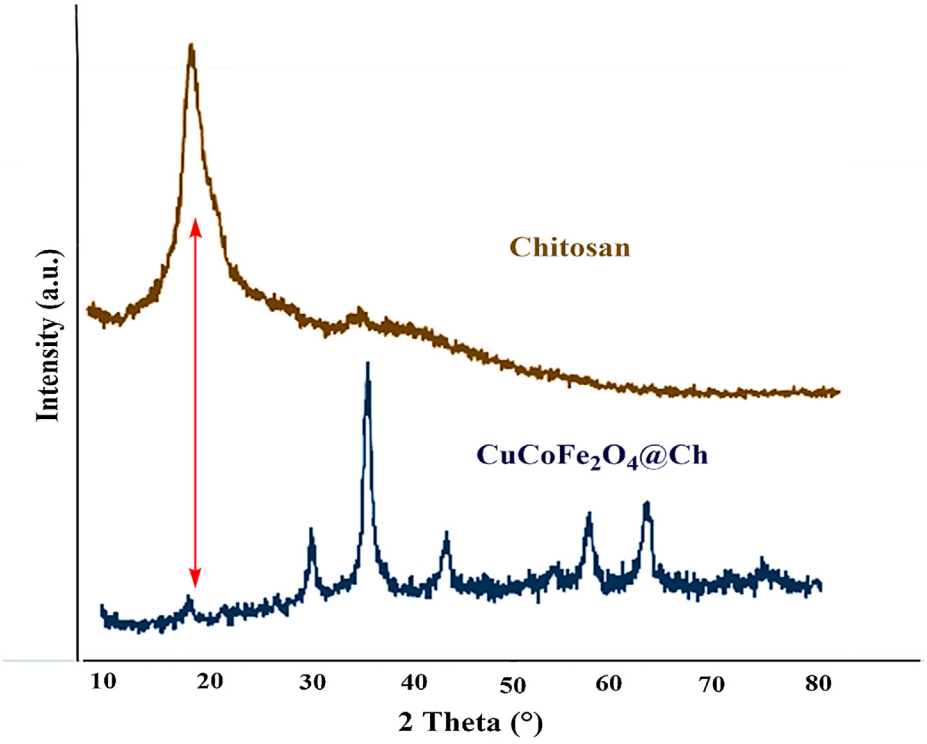

Fig. 6 The XRD pattern of $CuCoFe_2O_4$@Ch magnetic nanocomposite.

3.2.2. Effect of the initial concentration of TC

Concentration is one of the effective parameters in the adsorption process that has been investigated in this experiment. In this study, initial concentrations of 5, 10, 15, 20, and 30 mg/L were investigated. Fig. 11 depicts the effect of the initial TC concentration at various periods. According to this figure, the removal efficiency decreased from 91.19 to 53.68% when the TC concentration increased from 5 to 30 mg/L. Therefore, at a concentration of 5 mg/L, it exhibited the maximum removal efficiency. With a concentration increase from 5 to 30 mg/L, the adsorbent's adsorption capacity increased from 1.133 to 4.041 mg/g. The low dosage of adsorbent, as a result of which there was a less active site for TC adsorption on the adsorbent surface, is one of the causes of the reduction in efficiency with increasing concentration (Takdastan et al., 2016). On the other hand, TC will saturate the surface of the nano-sorbent faster at greater concentrations such that additional TC will no longer be adsorbed on a broad active surface, while the TC prefers to enter active sites inside the adsorbent. The adsorption rate of the TC is significantly lower than the surface sites in these locations, which in turn lowers TC adsorption efficiency (Ahamad et al., 2020; Gopal et al., 2020b). Debnath et al. investigated the removal of tetracycline using ZrO_2NPs nano-sorbent and found that the best effectiveness for tetracycline removal occurs at the lowest concentration (Debnath et al., 2020).

3.2.3. Effect of pH on TC adsorption

In nano-sorbent adsorption, pH is a highly essential element since it has a major influence on the charge of the nano-sorbent surface (negative or positive), and hence the optimum pH for enhancing TC adsorption is a topic. The pH influences the kind of adsorbent surface charge and the type of adsorbed charge, which is critical (Ahamad et al., 2020). In this experiment, the effect of pHs of 3.5, 5.5, 7.5, 9.5, and 11.5 on the rate of TC adsorption by $CuCoFe_2O_4$@Ch magnetic nano-sorbent was evaluated. As shown in Fig. 12a, with rising pH from 3.5 to 11.5, the TC uptake efficiency fell from 93.07% to 6.94% after 20 min. Considering the pH of the experiment and that the value of pK_a for TC at different pHs according to Fig. 12b is equal to 3.3, 7.69, and 9.69, therefore at pHs between 3.3 and 7.69, the charge of TC is both positive and negative (Chen and Huang, 2010). According to the measured pH_{zpc} of 6.15, the surface charge of the magnetic nano-sorbent $CuCoFe_2O_4$@Ch becomes positive at pHs below pH_{zpc} due to the presence of positively charged H^+ ions, and the surface charge of the magnetic nano-sorbent $CuCoFe_2O_4$@Ch becomes negative at higher pHs of pH_{zpc} due to negatively charged OH^- ions, therefore at pH 6.15, the electric charge of the adsorbent is zero, and there is no attraction or repulsion between the adsorbent and the tetracycline, and only the physical driving forces are involved in the absorption of the tetracycline (Fig. 12c) (Ahamad et al., 2020). Due to the effect of pH on the surface charge of the magnetic nano-sorbent $CuCoFe_2O_4$@Ch and pK_a of the antibiotic tetracycline, the forces of attraction and repulsion between TC and nano-sorbent are formed, resulting in acidic pHs where the nano-sorbent charge is positive and the TC charge is positively and negatively, there is an electrostatic attraction that better adsorbs TC on the nano-sorbent surface. A repulsive interaction is produced between the TC and the nano-sorbent surface at alkaline pHs when the nano-sorbent charge is negative and has the same name as the TC charge. As a result, the adsorp-

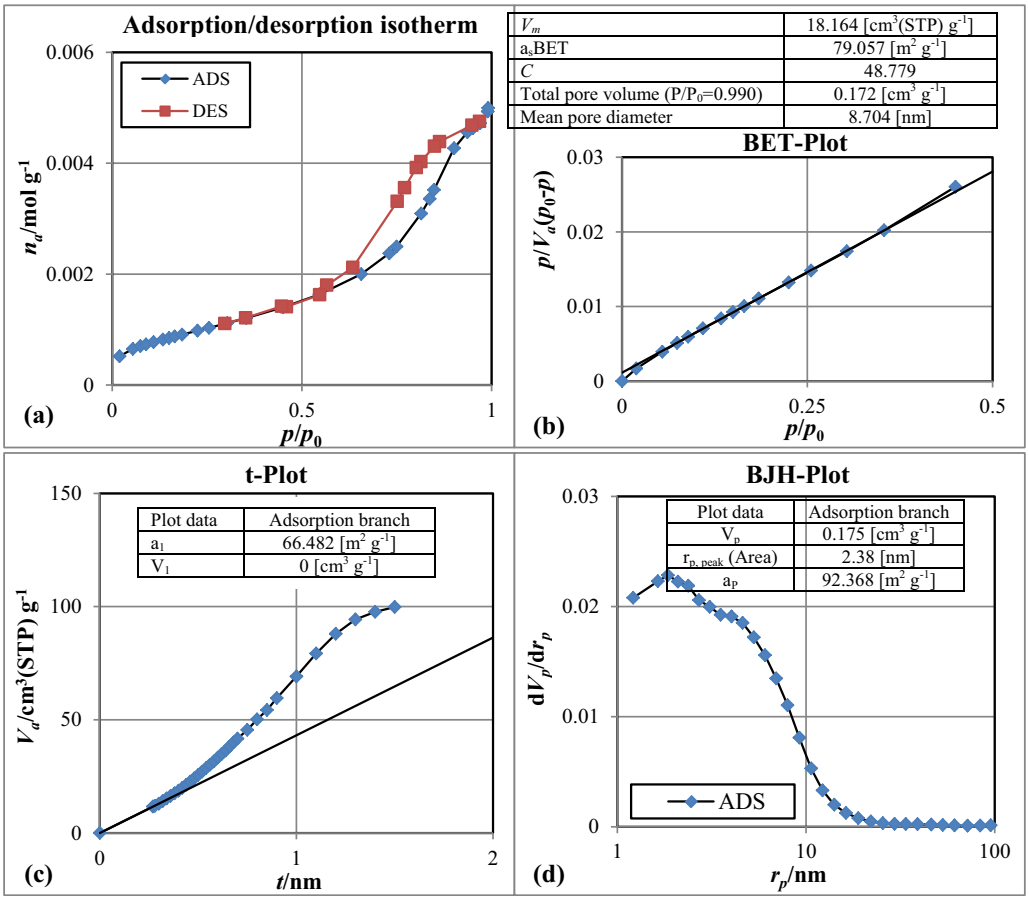

Fig. 7 Adsorption/desorption isotherm (a), BET surface area (b), t-Plot (c) and BJH surface area (d) of $CuCoFe_2O_4$@Ch magnetic nano-adsorbent.

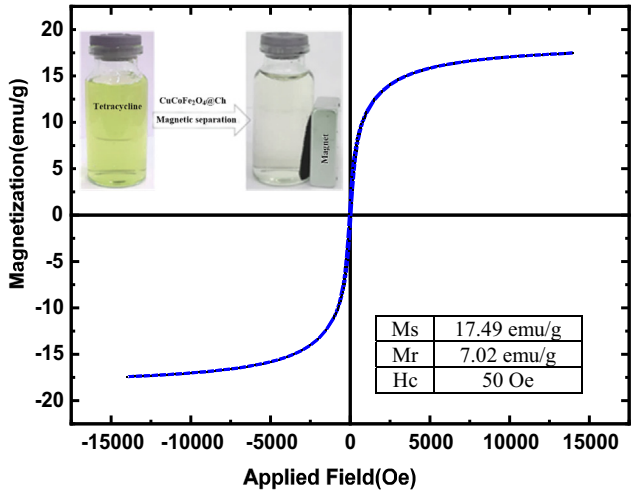

Fig. 8 VSM magnetization curve of $CuCoFe_2O_4$@Ch magnetic nano-adsorbent.

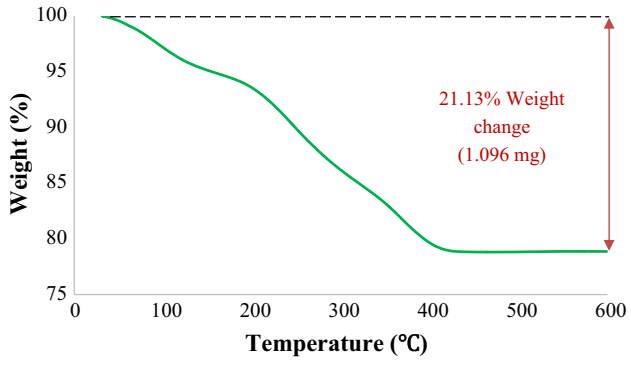

Fig. 9 The TGA pattern of $CuCoFe_2O_4$@Ch magnetic nanocomposite.

tion rate on the nano-sorbent surface drops (Malakootian et al., 2018b; Nasiri et al., 2021b). Nasiri et al. came to the same result when looking at the influence of pH on TC absorption, which decreases as pH rises (Nasiri et al., 2021b).

3.2.4. *Effect of temperature*

Fig. 13 shows the findings of the influence of temperature on the TC adsorption process by $CuCoFe_2O_4$@Ch magnetic nano-sorbent. Temperatures of 25, 30, 35, and 40 °C were examined in this study. According to the findings, the removal effectiveness of TC by $CuCoFe_2O_4$@Ch magnetic nano-sorbent fell from 93.07% to 85.31% at 20 min when the temperature was increased from 25 to 40°Celsius. As a consequence, the $CuCoFe_2O_4$@Ch magnetic nano adsorbent's

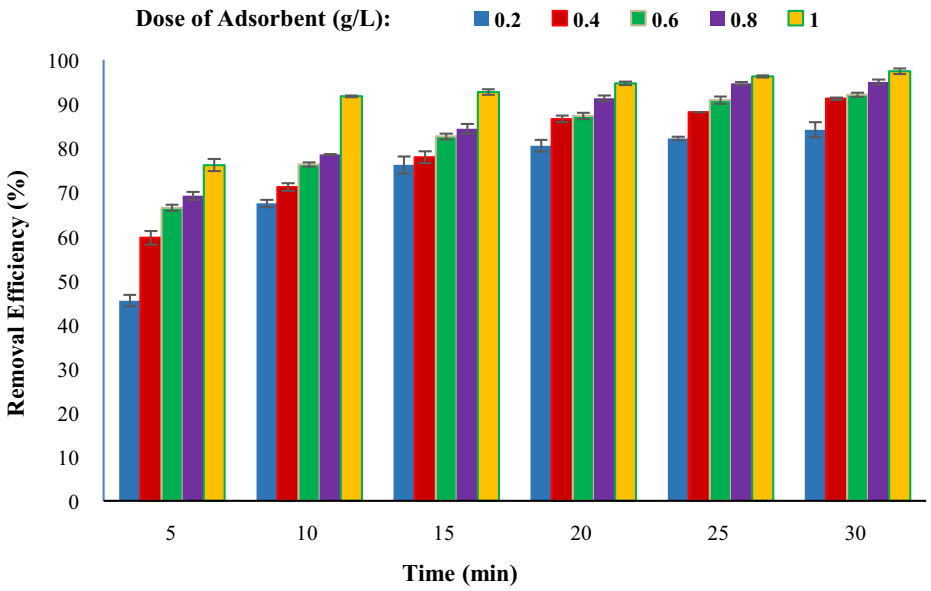

Fig. 10 Comparison of removal efficiency at a different adsorbent dose (g/L) (TC concentration 5 mg/L, temperature 25 °C, pH 4).

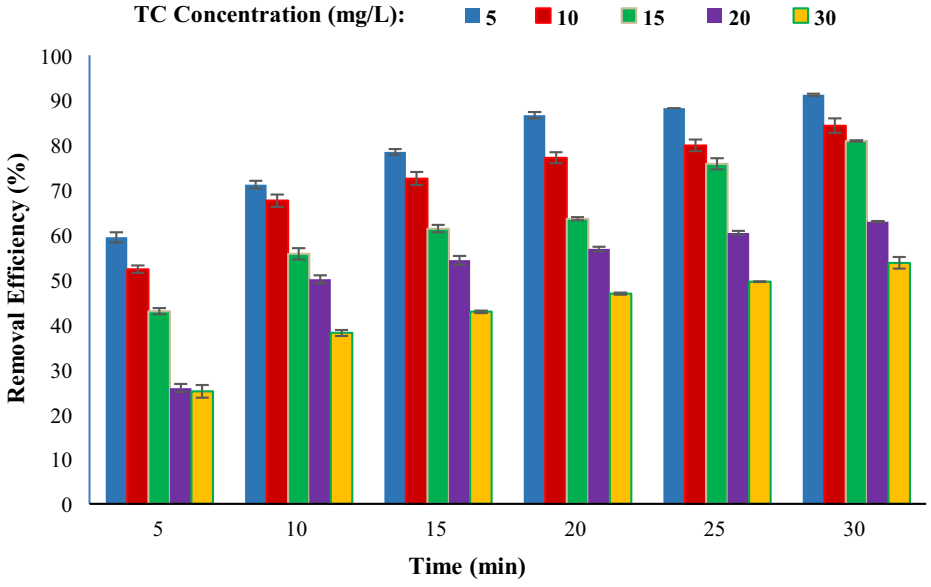

Fig. 11 Comparison of removal efficiency at different TC concentrations (mg/L) (dose of adsorbent 0.4 g/L, temperature 25 °C, pH 4).

optimal temperature for TC removal was 25 °C. Because the effectiveness of the TC adsorption process decreases with increasing temperature, it is evident that the removal of TC from the aqueous medium by this magnetic nano-sorbent was a spontaneous and exothermic reaction. By contrast, raising the temperature increased the solubility and mobility of TC on the adsorbent surface, which led to the dissociation from its adsorbent and desorbent surfacing. The inactivation or destruction of certain active adsorbent sites owing to high temperature may be the cause of this instability and increase in TC mobility at the adsorbent surface (Mohammed and Kareem, 2019; Song et al., 2017). Song et al. conducted a similar investigation on the adsorption of tetracycline. They also discovered that raising the temperature lowered tetracycline adsorption on the adsorbent surface (Song et al., 2017).

3.2.5. Adsorption isotherm models

The equilibrium adsorption isotherms must be known to build water and wastewater treatment systems based on the adsorption process. Three of the most prevalent models of adsorption processes are the Freundlich, Langmuir, and Temkin isotherms. Isotherm studies are used to estimate the number of pollutants adsorbed per unit weight of adsorbent, which defines the adsorbent's adsorption capacity (Malhotra et al., 2018; Batool et al., 2018). The adsorption of pollutants occurs as a single layer on the adsorbent surface in the Langmuir iso-

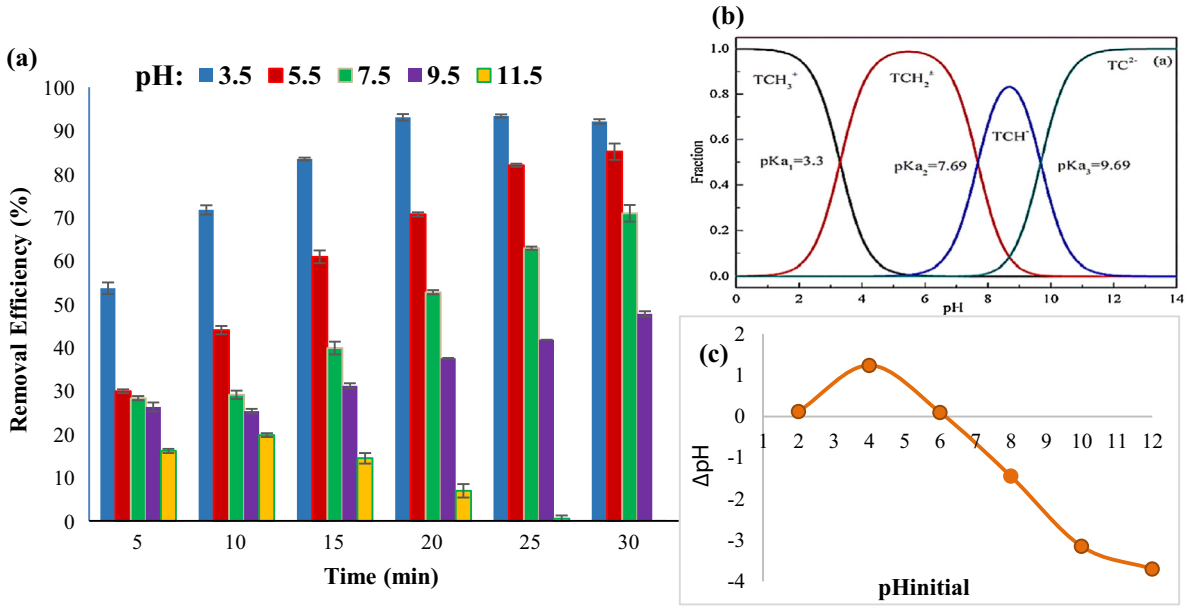

Fig. 12 Comparison of removal efficiency at different pHs (a), fractions of TC in different pHs (b), and the zero point of charge (pH_{zpc}) (c) (TC concentration 5 mg/L, temperature 25 °C, dose of adsorbent 0.4 g/L).

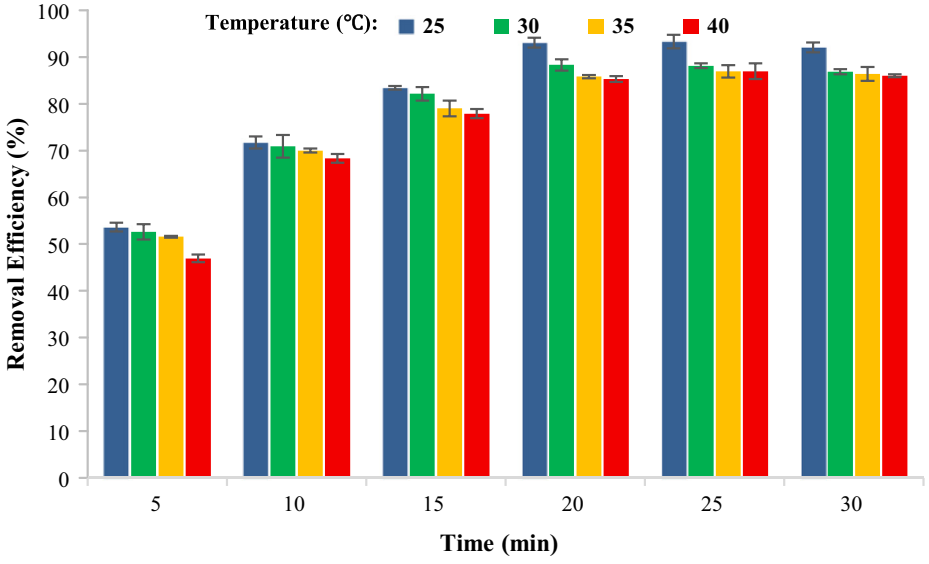

Fig. 13 Comparison of removal efficiency at different temperatures (TC concentration 5 mg/L, optimized pH 3.5, dose of adsorbent 0.4 g/L).

therm model. In this model, the intermolecular forces diminish as the distance from the adsorbent surface rises, and each contaminating molecule is adsorbed only on one active adsorbent site; on the other hand, the adsorbent surface in this model is considered homogenous (Afshin et al., 2021; Moghaddam et al., 2019). The adsorbent surface is heterogeneous in the Freundlich isotherm model, and pollutants are adsorbed in several layers on the adsorbent surface. On the other hand, the active sites on the adsorbent surface are distributed unevenly and have various adsorption energies (Meroufel et al., 2013; Pellicer et al., 2018). Using the equations below, the Langmuir isotherm (Eq.3) and Freundlich isotherm (Eq. (4)) were calculated, and their curves are presented in Fig. 14 (a-d).

$$\frac{C_e}{Q_e} = \frac{1}{Q_{max} K_L} + \frac{C_e}{Q_{max}} \tag{3}$$

$$\ln Q_e = \left(\frac{1}{n}\right) \ln C_e + \ln K_f \tag{4}$$

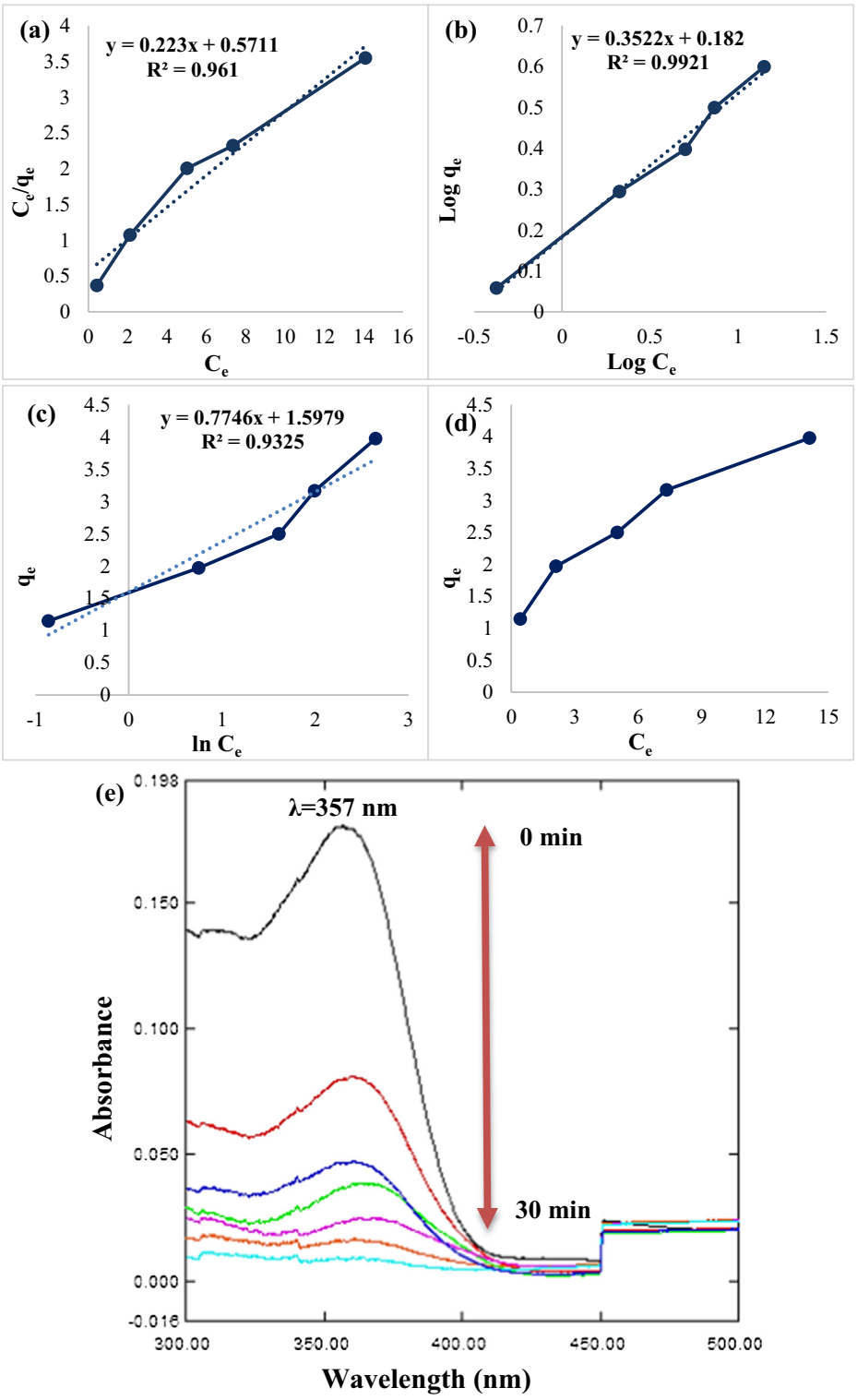

Fig. 14 The Langmuir isotherm (a), the Freundlich isotherm (b), Temkin isotherm (c), q_e vs. C_e (d) variation in UV–vis spectra of TC with reaction time (e) for the TC adsorption under optimal conditions (pH: 3.5, adsorbent dose: 0.4 g/L, and contact time: 20 min).

C_e is the TC equilibrium concentration in the solid phase (mg/g) and Q_{max} is the maximum adsorption (mg/g). K_L is the Langmuir adsorption equilibrium constant (1/mg), while K_f is the Freundlich constant (mg/g) $(L/mg)^{1/n}$. The adsorption rate is represented by the constant n (Nasseh et al., 2019).

The separation factor or equilibrium parameter R_L, which is used to predict whether the studied adsorption system is favorable or unfavorable, may be utilized to explain the basic characteristics of the Langmuir isotherm. It was defined using Eq. (5).

$$R_L = \text{QUOTE}\, R_L \frac{1}{(1 + K_L\ C_0\ )} \quad (5)$$

C_0 is the TC starting concentration (mg/L), while K_L is the Langmuir adsorption equilibrium constant (L/mg). The value of R_L indicates whether adsorption is unfavorable ($R_L > 1$), linear ($R_L = 1$), favorable ($0 < R_L < 1$), or irreversible ($R_L = 0$).

The Temkin isotherm considers the adsorbent-adsorbate interaction. According to this model, which excludes very higher and lower concentrations, the adsorption thermal diffusivity of all molecules may decline linearly rather than logarithmically. The linear formulation of the Temkin isotherm is shown in Eqs. (6) and (7) (Al-Trawneh et al., 2021).

$$qe = BTlnKT + BTlnCe \quad (6)$$

$$bT = (RT)/(BT) \quad (7)$$

The K_T represents the Temkin adsorption potential (L/g), while the B_T and b_T are constants. R and T are the universal gas constant and temperature, respectively.

According to the results of the study of the Langmuir and Freundlich isotherms in Table 1, the value of R^2 in the Freundlich isotherm is higher than Langmuir, so Freundlich is the dominant isotherm in the TC adsorption process, which has a multilayer adsorption mechanism on the heterogeneous adsorbent surface. Zhang et al. discovered that the tetracycline adsorption mechanism by the adsorbent fits the Freundlich isotherm model, indicating that this isotherm is prevalent in the adsorption process (Zhang et al., 2019).

3.2.6. TC adsorption kinetic study

Three *pseudo*-first-order, *pseudo*-second-order kinetic, and Intraparticle diffusion models were used to evaluate the rate of TC adsorption on $CuCoFe_2O_4$@Ch adsorbent under optimum circumstances in kinetic experiments. For kinetic adsorption studies, a variety of models are employed, but the most frequent and commonly used are *pseudo*-first-order and *pseudo*-second-order kinetics (Riahi et al., 2017; Yousefi et al., 2021). Adsorption kinetics study has looked at the rate of adsorption processes that are used to determine, model, and conduct processes in the reaction medium (Baghapour et al., 2014). The *pseudo*-first-order kinetics (Eq.6) and *pseudo*-second-order kinetics (Eq. (7)) were calculated using the equations below.

$$log(qe - qt) = logqe - K1t \quad (8)$$

The quantity of adsorbate on the adsorbent (mg/g) is presented by q_t and q_e, the time of adsorption (t), and the *pseudo*-first-order adsorption rate constant (1/min) is represented by K_1. A graph of log (q_e-q_t) against t was used to determine the R^2 coefficient and the value of the constant K_1.

$$\frac{t}{q_t} = \frac{1}{K_2 q_e^2} + \frac{1}{q_e} t \quad (9)$$

A *pseudo*-second-order adsorption rate constant is K_2 (g/(mg.min)). A graph of t/q_t versus t was used to calculate the speed parameters. The slope and y-intercept of the figure were used to compute the values of q_e and K_2 (Nasseh et al., 2019).

When graphing the molecules adsorbed vs the square root of the contact period, a straight line is formed, indicating that intraparticle diffusion is level-limiting in the adsorption process. One of the most widely utilized intraparticle diffusion formulas for adsorption processes was developed by Weber and Morris (1963) (Ofomaja et al., 2020; Weber Jr and Morris, 1963).

$$q_t = k_i t^{0.5} + C \quad (10)$$

where k_i denotes the intraparticle diffusion rate constant (g/mg.min) and C denotes the boundary layer influence or surface adsorption, with the sharper the intercept, the greater the effect of surface adsorption in the level-limiting phase. Whenever the kinetic analysis was done utilizing the intraparticle diffusion model, the curve could not cross thru the origin, indicating that intraparticle diffusion was not the dominant level-limiting mechanism.

The adsorption process is more closely followed by the *pseudo*-second-order kinetic because the values of R^2 in Table 2 are greater than the *pseudo*-first-order kinetic. As a result, at a concentration of 5 mg/L, the best model for the TC adsorption process was *pseudo*-second-order kinetic, with $R^2 = 0.993$. Nasiri et al. used the $CoFe_2O_4$@MC adsorbent to investigate the adsorption kinetics of tetracycline. They concluded that the adsorption of tetracyclines follows a *pseudo*-second-order kinetic model (Nasiri et al., 2021b). Fig. 14(e) shows the spectra of variations in TC removal over time and under ideal circumstances (pH: 3.5, adsorbent dose: 0.4 g/L, and contact time: 20 min). TC has a 357 nm absorption peak. The intensity of absorption reduced as the TC content dropped.

3.2.7. Thermodynamic evaluation of the TC adsorption process

The impact of temperatures of 25, 30, 35, and 40 degrees Celsius on the tetracycline adsorption process on $CuCoFe_2O_4$@-Ch nano-sorbent under optimum circumstances was studied

Table 1 The Langmuir, Freundlich, and Temkin isotherm parameters (pH: 3.5, adsorbent dose: 0.4 g/L, initial concentration: 5 mg/L, and temperature: 25 °C).

Adsorbent	Freundlich isotherm			Langmuir isotherm				Temkin		
$CuCoFe_2O_4$@Ch	R^2	K_f[(mg/g) (1/mg)]	1/n	R^2	R_L	q_m (mg/g)	K_L (L/mg)	R^2	B_1	K_t (L/mg)
	0.992	1.521	0.352	0.961	0.339 0.204 0.146 0.114 0.079	4.484	0.391	0.933	0.775	7.869

Table 2 The kinetic parameters (pH: 3.5, adsorbent dose: 0.4 g/L, and contact time: 20 min).

Adsorbent	*Pseudo*-first-order kinetic model			*Pseudo*-second-order kinetic model			Intraparticle kinetic model		
$CuCoFe_2O_4$@Ch	R^2	K_1 (1/min)	q_e (mg/g)	R^2	K_2 (g/mg.min)	q_e (mg/g)	R^2	K_P (mg/g. min^{-5})	C (mg/g)
	0.902	−0.855	1.127	0.993	0.267	3.936	0.885	0.149	0.394

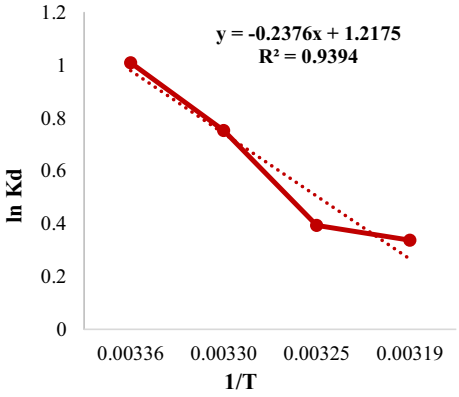

Fig. 15 The thermodynamic for the TC adsorption under optimal conditions (pH:3.5, adsorbent dose:0.4 g/L, initial concentration:5 mg/L, and temperature:25 °C).

in thermodynamic experiments. In thermodynamic research, the three major elements of Gibbs free energy (ΔG), enthalpy changes (ΔH), and entropy changes (ΔS) were examined. The thermodynamic curve for TC adsorption is shown in Fig. 15. To calculate Gibbs free energy changes (ΔG) (Eq. (8)), standard enthalpy changes (ΔH), and standard entropy changes (ΔS) (Eq. (9)), the following equations were employed.

$$\Delta G = -RTlnk_d \tag{11}$$

$$lnK_d = \frac{\Delta S}{R} - \frac{\Delta H}{RT} \tag{12}$$

ΔG is for Gibbs free energy changes, R refers for 8.314 J/mol/K universal gas constant, T refers for temperature (K), K_d refers for thermodynamic equilibrium, ΔS refers for standard entropy (kJ/mol), and ΔH refers for standard enthalpy changes (KJ/mol). After determining the thermodynamic equilibrium constant for Gibbs free energy at various temperatures, a graph of lnK_d versus $1/T$ was produced, and the values of ΔS and ΔH were computed using their slope and origin-intercept (Nasseh et al., 2019).

Considering the negative values of enthalpy changes (ΔH = −1.975 kJ/mol) and positive values of entropy changes (ΔS = 10.122 j/mol.k) in Table 3, respectively, show that the adsorption process is exothermic and the irregularity increases with increasing temperature, which results in increased motility of TC molecules in solution disrupts the absorption process. Gibb's free energy (ΔG = −4.992 kJ/mol) indicates that the TC adsorption process is spontaneous and based on the results, it was found that the value of Gibb's free energy decreases with increasing temperature, so it can be said that the TC adsorption process by $CuCoFe_2O_4$@Ch adsorbent is spontaneous. It's a sort of physical adsorption since the efficacy of the adsorption process decreases with rising temperature. If the chemical adsorption process worked in the opposite direction, it would be due to chemical adsorption taking energy, which increases with temperature and performance. Physical and chemical adsorption always are there, however owing to increasing temperatures and decreased efficiency, physical adsorption gains precedence (Bering et al., 1972; Darwish et al., 2019). Liu et al. found in research on the adsorption of tetracycline on this adsorbent that the adsorption process of tetracycline on this adsorbent is a spontaneous reaction with negative Gibbs free energy values, and that the reaction was exothermic owing to the negative amount of enthalpy changes (Liu et al., 2020).

Table 3 The thermodynamic parameters (pH: 3.5, adsorbent dose: 0.4 g/L, initial concentration:5 mg/L and temperature: 25 °C).

T (k)	ΔG (kJ/mol)	ΔH (kJ/mol)	ΔS (j/mol.k)
298	−4.992	−1.975	10.122
303	−5.043		
308	−5.093		
313	−5.144		

3.3. Comparison with other adsorbents to TC adsorption

This adsorbent has a high removal efficiency and is more cost-effective and practical than other adsorbents, as indicated in Table 4.

3.4. Reusability and chemical stability of $CuCoFe_2O_4$@Ch

From an economic standpoint, the regeneration research of synthesized adsorbents is essential. TC adsorption was evaluated using a batch adsorption experiment. The adsorbent was separated by a magnet and regenerated using EtOH/H_2O in a 1:1 ratio during usage under the following circumstances (pH: 3.5, adsorbent dose: 0.4 g/L, starting concentration: 5 mg/L, and temperature: 25 °C), then rinsed several times with deionized water and dried in a 70 °C oven. Once the adsorbent had dried, it was utilized for the next cycle. To assess the adsorbent's reusability potential, the adsorption–desorption method was repeated up to four times under optimum circumstances. Fig. 16a shows that the removal effectiveness fell from 93.07% to 82.16% after four cycles, however, it was almost maintained after four cycles. The irreversible occupancy of the active adsorbent sites might explain the decline in TC removal effectiveness after four cycles of reduction and reuse (Guo et al., 2017; Nasiri et al., 2021b; Bao et al., 2018; Mmelesi et al., 2020). After the four cycles, the chemical stabil-

Table 4 Comparison of $CuCoFe_2O_4$@Ch with other adsorbents to TC adsorption.

No.	Adsorbent	Dose of adsorbent (g/L)	TC concentration (mg/L)	Contact time (min)	Efficiency (%)	Ref.
1	Fe_3O_4@SiO_2-Chitosan/ Graphene oxide	0.4	44.4	480	85.7	(Foroughi et al., 2020)
2	ZrO_2NPs	1	100	15	92.57	(Debnath et al., 2020)
3	Fe_3O_4@C	0.5	30	60	73.3	(Soares et al., 2019)
4	LDH	6	60	150	82	(Soori et al., 2016)
5	CHT MPNs	0.5	50	150	78.8	(Raeiatbina and Açıkelb, 2017)
6	MIL-101(Cr)	0.5	100	540	82.9	(Jin et al., 2019)
7	$CuCoFe_2O_4$@Ch	0.4	5	20	93.07	This work

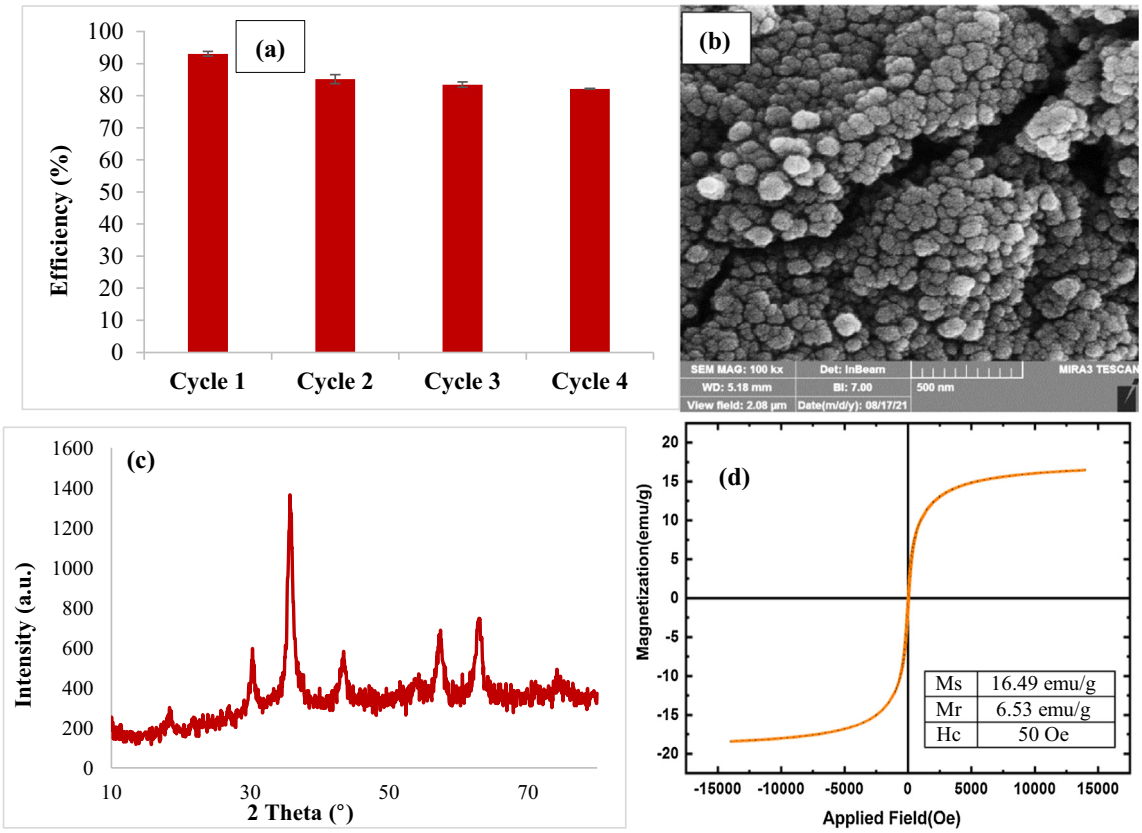

Fig. 16 Regeneration (a), FESEM image (b), XRD analysis (c) and VSM (d) of $CuCoFe_2O_4$@Ch magnetic nano-adsorbent after four recycling cycles (pH:3.5, adsorbent dose:0.4 g/L, initial concentration:5 mg/L and temperature:25 °C).

ity of the adsorbent was evaluated using FESEM, XRD, and VSM techniques (Fig. 16b-d). According to FESEM results, the adsorbent's morphological characteristics were retained after the fourth cycle. After four cycles of usage and regeneration, there was no significant change in the position of 2 Theta in the XRD analysis pattern, however, the quantity of peak diffraction intensity decreased somewhat and the adsorbent's crystal structure was preserved. The magnetic property of the adsorbent did not change appreciably after four cycles of use and regeneration. Ms (16.49 emu/g) and the magnetic property of $CuCoFe_2O_4$@Ch were both reduced somewhat. As a result, this adsorbent is chemically stable and easy to recover. After the process in an aqueous medium, the concentrations of Cu (wavelength 324.8 nm), Co (wavelength 240.7 nm), and Fe (wavelength 248.3 nm) were determined utilizing an Atomic Absorption Spectrophotometer (AAS, CTA-3000) to evaluate the chemical stability of $CuCoFe_2O_4$@Ch. The amounts of Cu: 2 mg L^{-1}, Fe: 0.4 mg L^{-1}, and Co: below the detection limit of AAS were obtained using this instrument, indicating that this nano-adsorbent has adequate chemical stability.

3.5. Adsorption mechanism

The adsorption mechanism of TC by the $CuCoFe_2O_4$@Ch magnetic adsorbent is shown in Fig. 17a, and the comparative FTIR of $CuCoFe_2O_4$@Ch before and after TC adsorption is shown in Fig. 17b.

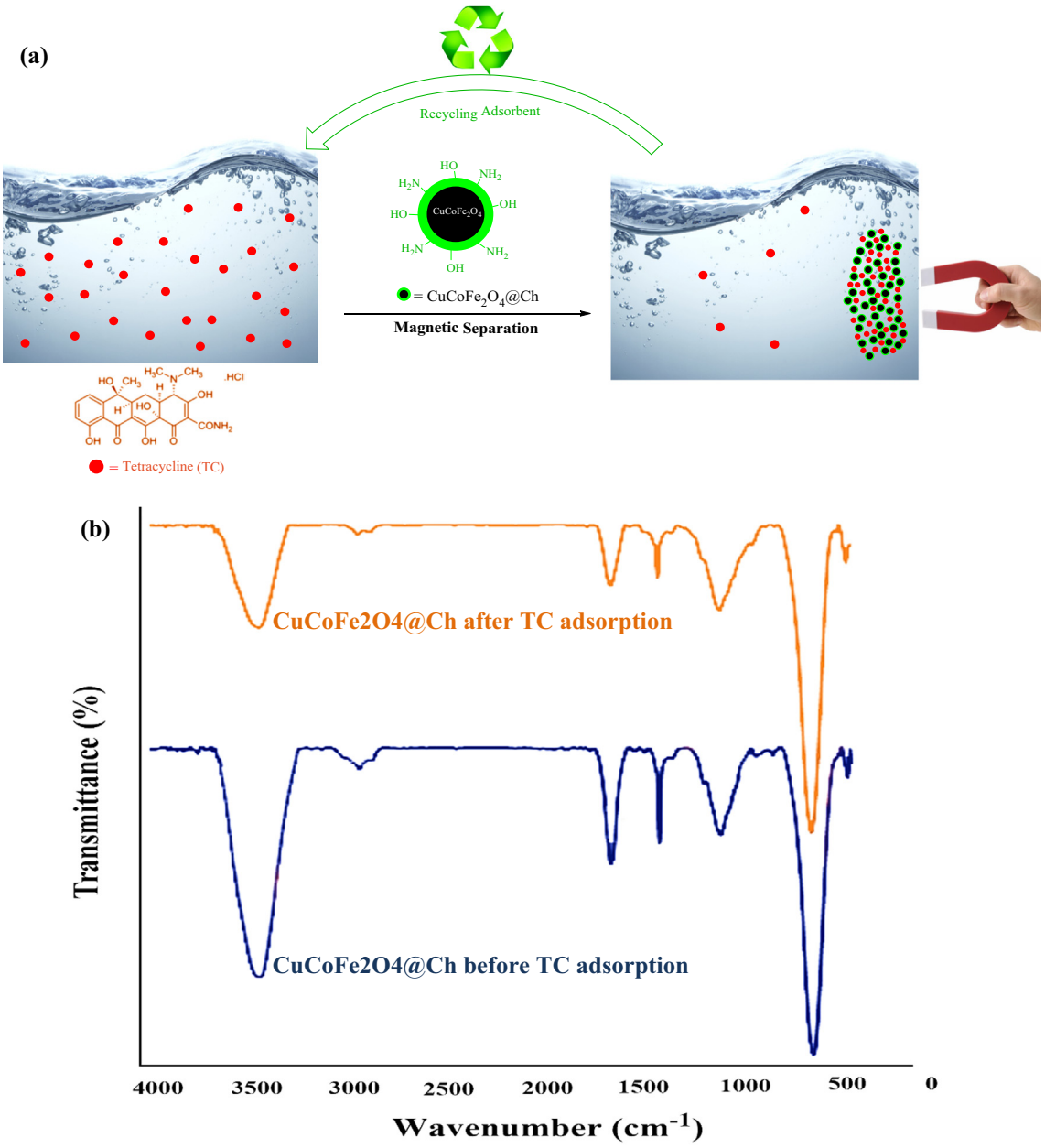

Fig. 17 Adsorption mechanism (a), FTIR of $CuCoFe_2O_4$@Ch before and after TC adsorption (b).

The FTIR spectra, though, indicate modest changes due to the TC's surface binding. The peak intensity of the functional groups O—H stretching at 3431 cm^{-1}, CH_2 stretching at 2923 cm^{-1}, NH primary amine bends at 1633 cm^{-1}, C—O in the primary alcoholic group at 1383 cm^{-1}, and NH_2 free amino group at 1069 cm^{-1} lowered as a consequence of the FTIR analysis, and these functional groups shifted toward lower wavelengths of the O—H stretching vibration band at 3429 cm^{-1}, NH primary amine bends at 1622 cm^{-1}, and NH_2 free amino group at 1065 cm^{-1}, indicating that they were engaged in the tetracycline adsorption mechanism. These changes, together with the results of desorption experiments, led to the conclusion that the $CuCoFe_2O_4$@Ch surfaces' hydroxyl and etheric sites are involved in TC sequestration, resulting in the formation of inner-sphere surface complexes.

Furthermore, at ideal conditions, the efficiency of $CuCoFe_2O_4$@Ch and $CuCoFe_2O_4$ for TC adsorption was evaluated (Fig. 18a). $CuCoFe_2O_4$@Ch and $CuCoFe_2O_4$ achieved removal performance of 93.07 % and 76 %, respectively, according to the results. $CuCoFe_2O_4$@Ch had a much higher removal efficiency than $CuCoFe_2O_4$ after 20 min. FESEM images of $CuCoFe_2O_4$@Ch and $CuCoFe_2O_4$ are also shown in Fig. 18 b-c. $CuCoFe_2O_4$ was synthesized without Ch. The $CuCoFe_2O_4$ sample has more aggregated than the $CuCoFe_2O_4$@Ch synthesized sample. $CuCoFe_2O_4$@Ch particles synthesized with Ch aggregated significantly less than $CuCoFe_2O_4$ nanoparticles synthesized without Ch, according to FESEM images. This observation might be explained in one of two ways. The existence of Ch during the production of $CuCoFe_2O_4$@Ch, which has a larger surface area than

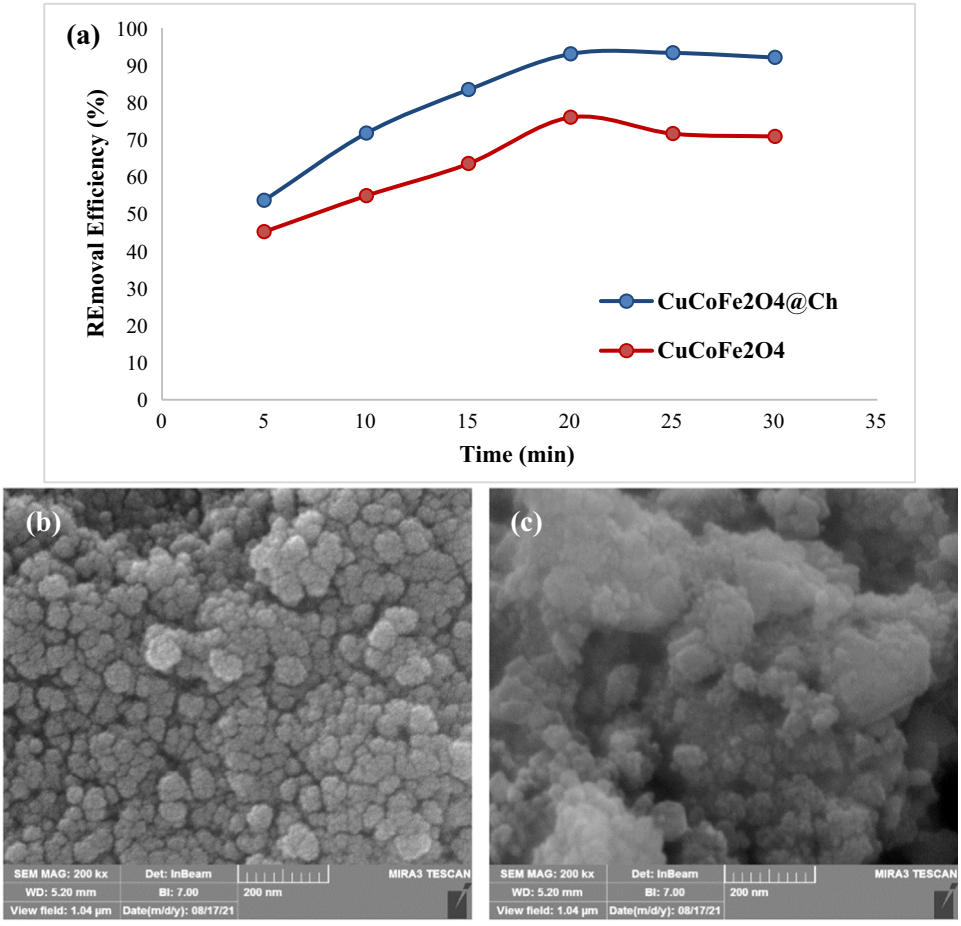

Fig. 18 The performance comparison of $CuCoFe_2O_4$@Ch and $CuCoFe_2O_4$ under optimal conditions for adsorption of TC (TC concentration = 5 mg/L, pH = 3.5, adsorbent dose = 0.4 g/L, and temperature = 25 °C) (a), FESEM images of $CuCoFe_2O_4$@Ch (b) and $CuCoFe_2O_4$ (c).

$CuCoFe_2O_4$, might be the initial reason. The magnetic nanoadsorbent surface area is enhanced, leading to a large adsorbent surface area contacting TC and an improved TC adsorption efficiency. Hydroxyl (OH) and amine (NH_2) groups of Ch also produce electrostatic contact between TC and $CuCoFe_2O_4$@Ch surface. As a consequence, a greater number of TC molecules are deposited on the adsorbent's surface, resulting in increased interaction and improved adsorption properties.

3.6. Investigation of process efficiency on real wastewater

In this work, a novel magnetic nanocomposite adsorbent $CuCoFe_2O_4$@Ch was used to remove TC from a real sample, and the removal efficiency of TC was compared to the removal efficiency of TC from a synthetic sample. The real sample was collected from the Kerman University of Medical Sciences' wastewater treatment facility, and the physical and chemical properties of this wastewater are presented in Table 5.

To assess the method on a real sample, the sample was spiked with 5 mg/L of TC and the sample parameters were modified to the optimal on a synthetic sample. After the procedure, the sample is centrifuged to remove turbidity from the real wastewater and measure the TC concentration in the sample. Under optimal conditions (pH 3.5, TC concentration 5 mg/L and adsorbent dosage 0.4 g/L, contact duration 20 min, and temperature 25 °C), the removal efficiency of TC from the real sample was roughly equivalent to 67%, suggesting high removal efficiency of TC from the real sample by this absorbent. While, in the synthetic sample, the removal effectiveness of TC was equivalent to 93.07%. The removal effectiveness of TC in the real sample of wastewater was lower than that of the synthetic sample, according to the findings.

Table 5 Characteristics of real wastewater collected from Kerman University of Medical Sciences.

Parameter	Amount
BOD_5	8 mg/L
COD	26.1 mg/L
TSS	78 mg/L
TDS	1194 mg/L
TKN	1.82 mg/L
Phosphate	38.38 mg/L
Nitrate	1.4 mg/L
Sulfate	134.5 mg/L
pH	7.38
TC	5 mg/L

This loss in efficiency can be achieved owing to the existence of soluble organic and ionic matter in the real wastewater sample, simultaneous adsorption on the adsorbent surface of competitive pollutants, the complex wastewater matrix, and competition for compounds adsorption such as organic suspended material, the sulfate anions and other chemical compounds (Okoli and Ofomaja, 2019; Dolatabadi et al., 2020). On the other hand, smaller molecules are most likely to bind to the adsorbent surface groups, filling the active sites on the nanocomposite surface and lowering the TC adsorption capacity of the surface (Malakootian et al., 2019f). Malakootian et al. investigated the removal of metronidazole using the $CoFe_2O_4$/Activated Carbon@Chitosan adsorbent and found that the removal efficiency of metronidazole in a real sample is lower than in a synthetic sample (Malakootian et al., 2019f).

4. Conclusion

$CuCoFe_2O_4$@Ch magnetic nanocomposite was produced for the first time in this work and utilized as a magnetic nanocomposite to remove TC. Chitosan enhanced the adsorbent's structural characteristics and efficiency. The influence of four key variables on TC adsorption by $CuCoFe_2O_4$@Ch magnetic nanocomposite, including pH, starting TC concentration, adsorbent dose, and temperature, was also investigated and improved. According to the data, the best TC removal effectiveness was 93.07% under ideal circumstances (TC initial concentration 5 mg/L, pH 3.5, adsorbent dose 0.4 g/L, and temperature 25 °C). Under ideal circumstances, the $CuCoFe_2O_4$@Ch magnetic nanocomposite could adsorb 67% of TC from real wastewater. The adsorbent still exhibits a removal efficiency of about 82.16% after four cycles of use and recovery, which is adequate. The TC adsorption process in this adsorbent is governed by the Freundlich isotherm and *pseudo*-second-order kinetics. This process is exothermic, which implies that the efficiency of TC removal decreases as the temperature rises. According to the findings, the $CuCoFe_2O_4$@Ch magnetic nanocomposite has a high potential for adsorbing TC from both synthetic and real wastewater. The environmental importance of nano-adsorbent interactions should be the focus of future research. There is a need to look at a wide range of microorganism species, change the emphasis to more ecologically relevant exposure conditions, and establish a thorough perspective of antibiotic exposure and ecological processes, and food supply. Understanding the potential for antibiotic trophic transmission is crucial to achieving this.

Declaration of Competing Interest

The authors declare that they have no known competing financial interests or personal relationships that could have appeared to influence the work reported in this paper.

Acknowledgments

This research with project number 400000390 and IR.KMU.REC.1400.497 ethic approval cod was conducted in the Student Research Committee of Kerman University of Medical Sciences. This research was supported by the Vice-Chancellor for Research and Technology of Kerman University of Medical Sciences.

Funding

This work was supported by the Kerman University of Medical Sciences, Kerman, Iran.

References

Abbasi, S., Turner, A., Hoseini, M., Amiri, H., 2021. Microplastics in the Lut and Kavir deserts, Iran. Environ. Sci. Technol. 55, 5993–6000.

Afshin, S., Rashtbari, Y., Vosough, M., Dargahi, A., Fazlzadeh, M., Behzad, A., Yousefi, M., 2021. Application of Box-Behnken design for optimizing parameters of hexavalent chromium removal from aqueous solutions using Fe3O4 loaded on activated carbon prepared from alga: kinetics and equilibrium study. J. Water Process Eng. 42, 102113.

Aghdasinia, H., Meshinchi, P., Peighambardoust, S.J., Zarei, M., Rahbari Asiabi, H., Mohammadian Soudmand, A.R., 2019. A Survey on the Adsorption Process for the Removal Pharmaceutical Pollution from Aqueous Solutions and Wastewater. J. Water Wastewater Sci. Eng. 4, 34–50.

Ahamad, T., Naushad, M., Al-Shahrani, T., Al-Hokbany, N., Alshehri, S.M., 2020. Preparation of chitosan based magnetic nanocomposite for tetracycline adsorption: Kinetic and thermodynamic studies. Int. J. Biol. Macromol. 147, 258–267.

Al-Trawneh, S.A., Jiries, A.G., Alshahateet, S.F., Sagadevan, S., 2021. Phenol removal from aqueous solution using synthetic V-shaped organic adsorbent: Kinetics, isotherm, and thermodynamics studies. Chem. Phys. Lett. 781, 138959.

Alizadeh, B., Delnavaz, M., Shakeri, A., 2017. Treatment of Synthetic Wastewater Containing of Cd (II) Using Novel Magnetic EDTA/Chitosan/TiO2 Nanocomposite. J. Environ. Health Eng. 4, 289–298.

Altintig, E., Kabadayi, O., Bozdag, D., Altundag, S., Altundag, H., 2022. Artificial neural network mathematical modeling of methyl violet removal with chitosan-coated clinoptilolite. Desalination Water Treatment 250, 252–265.

Amiri, H., Martinez, S.S., Shiri, M.A., Soori, M.M., 2022. Advanced oxidation processes for phthalate esters removal in aqueous solution: a systematic review. Rev. Environ. Health.

Arica, T.A., Ayas, E., Arica, M.Y., 2017. Magnetic MCM-41 silica particles grafted with poly (glycidylmethacrylate) brush: modification and application for removal of direct dyes. Microporous Mesoporous Mater. 243, 164–175.

Arica, T.A., Kuman, M., Gercel, O., Ayas, E., 2019. Poly (dopamine) grafted bio-silica composite with tetraethylenepentamine ligands for enhanced adsorption of pollutants. Chem. Eng. Res. Des. 141, 317–327.

Ariga, K., Vinu, A., Yamauchi, Y., Ji, Q., Hill, J.P., 2012. Nanoarchitectonics for Mesoporous Materials. Bull. Chem. Soc. Jpn. 85, 1–32.

Asgari, E., Sheikhmohammadi, A., Yeganeh, J., 2020. Application of the Fe3O4-chitosan nano-adsorbent for the adsorption of metronidazole from wastewater: Optimization, kinetic, thermodynamic and equilibrium studies. Int. J. Biol. Macromol. 164, 694–706.

Aslan, S., Yalçin, K., Hanay, Ö., Yildiz, B., 2016. Removal of tetracyclines from aqueous solution by nanoscale Cu/Fe bimetallic particle. Desalin. Water Treat. 57, 14762–14773.

Atesa, A., Altintigb, E., Demirelc, H., Yilmaza, M., 2017. Comparative study on adsorptive removal of Cu, Pb, Zn heavy metals by modified perlite composites. Desalination Water Treatment 98, 244–253.

Baghapour, M.A., Pourfadakari, S., Mahvi, A.H., 2014. Investigation of Reactive Red Dye 198 removal using multiwall carbon nanotubes in aqueous solution. J. Ind. Eng. Chem. 20, 2921–2926.

Balarak, D., Khatibi, A.D., Chandrika, K., 2020. Antibiotics removal from aqueous Solution and pharmaceutical wastewater by adsorption process: A review. Int. J. Pharmaceut. Investigat. 10, 106–111.

Bao, J., Zhu, Y., Yuan, S., Wang, F., Tang, H., Bao, Z., Zhou, H., Chen, Y., 2018. Adsorption of tetracycline with reduced graphene oxide decorated with MnFe 2 O 4 nanoparticles. Nanoscale Res. Lett. 13, 1–8.

Batool, F., Akbar, J., Iqbal, S., Noreen, S., Bukhari, S.N.A., 2018. Study of isothermal, kinetic, and thermodynamic parameters for adsorption of cadmium: an overview of linear and nonlinear approach and error analysis. Bioinorganic Chem Appl. 2018.

Bayramoglu, G., Arica, M.Y., 2021. Grafting of regenerated cellulose films with fibrous polymer and modified into phosphate and sulfate groups: application for removal of a model azo-dye. Colloids Surf., A 614, 126173.

Bering, B., Dubinin, M., Serpinsky, V., 1972. On thermodynamics of adsorption in micropores. J. Colloid Interface Sci. 38, 185–194.

Chang, S., Zhang, Q., Lu, Y., Wu, S., Wang, W., 2020. High-efficiency and selective adsorption of organic pollutants by magnetic CoFe2O4/graphene oxide adsorbents: Experimental and molecular dynamics simulation study. Sep. Purif. Technol. 238, 116400.

Chavoshani, A., Amin, M.M., Asgari, G., Seidmohammadi, A., Hashemi, M., 2018. Microwave/hydrogen peroxide processes. Advanced Oxidation Processes for Waste Water Treatment. Elsevier.

Chen, W.-R., Huang, C.-H., 2010. Adsorption and transformation of tetracycline antibiotics with aluminum oxide. Chemosphere 79, 779–785.

CRINI, G., 2005. Recent developments in polysaccharide-based materials used as adsorbents in wastewater treatment. Progress in Polymer Science (Oxford) 30, 38–70.

Dai, Y., Liu, M., Li, J., Yang, S., Sun, Y., Sun, Q., Wang, W., Lu, L., Zhang, K., Xu, J., 2020. A review on pollution situation and treatment methods of tetracycline in groundwater. Sep. Sci. Technol. 55, 1005–1021.

Darwish, A., Rashad, M., Al-Aoh, H.A., 2019. Methyl orange adsorption comparison on nanoparticles: Isotherm, kinetics, and thermodynamic studies. Dyes Pigm. 160, 563–571.

Datta, D., Kerkez Kuyumcu, Ö., Bayazit, Ş.S., Abdel Salam, M., tta et al. 2017. Adsorptive removal of malachite green and Rhodamine B dyes on Fe3O4/activated carbon composite. J. Dispersion Sci. Technol. 38, 1556–1562.

Debnath, B., Majumdar, M., Bhowmik, M., Bhowmik, K.L., Debnath, A., Roy, D.N., 2020. The effective adsorption of tetracycline onto zirconia nanoparticles synthesized by novel microbial green technology. J. Environ. Manage. 261, 110235.

DE CARVALHO OLIVEIRA, G., FILHO, G. R., VIEIRA, J. G., DE ASSUNÇÃO, R. M. N., DA SILVA MEIRELES, C., CERQUEIRA, D. A., DE OLIVEIRA, R. J., SILVA, W. G. & DE CASTRO MOTTA, L. A. 2010. Synthesis and application of methylcellulose extracted from waste newspaper in CPV-ARI Portland cement mortars. *J. Appl. Polym. Sci.* 118, 1380–1385.

Dolatabadi, M., Mehrabpour, M., Esfandyari, M., Ahmadzadeh, S., 2020. Adsorption of tetracycline antibiotic onto modified zeolite: Experimental investigation and modeling. MethodsX 7, 100885.

Dutta, V., Sharma, S., Raizada, P., Hosseini-Bandegharaei, A., Gupta, V.K., Singh, P., 2019. Review on augmentation in photocatalytic activity of CoFe2O4 via heterojunction formation for photocatalysis of organic pollutants in water. J. Saudi Chem. Soc. 23, 1119–1136.

EL-SAYED, A., 2002. Influence of zinc content on some properties of Ni–Zn ferrites. Ceram. Int. 28, 363–367.

Fadaei, S., Moghadam, F.N., Hashemi, M., Pourzamani, H., 2017. BTEX removal from aqueous solution by modified multi-walled carbon nanotubes with ozone. Anuario do Instituto de Geociencias 40, 235–242.

Fatehi, M.H., Shayegan, J., Zabihi, M., 2018. A review of methods for removing heavy metal from aqueous media. Iranian J. Ecohydrol. 5, 855–874.

Fernandes Queiroz, M., Melo, K.R.T., Sabry, D.A., Sassaki, G.L., Rocha, H.A.O., 2015. Does the use of chitosan contribute to oxalate kidney stone formation? Mar. Drugs 13, 141–158.

Foroughi, M., Azqhandi, M.H.A., Kakhki, S., 2020. Bio-inspired, high, and fast adsorption of tetracycline from aqueous media using Fe3O4-g-CN@ PEI-β-CD nanocomposite: Modeling by response surface methodology (RSM), boosted regression tree (BRT), and general regression neural network (GRNN). J. Hazard. Mater. 388, 121769.

GOLKARAMI, A., KAVIANI, RAD, 2017. The effect of limited water resources on hydropolitic tensions (Case Study: Iran's central catchment with emphasis on Zayandehrood basin). Geogr. Environ. Plann. 28, 113–134.

Gopal, G., Alex, S.A., Chandrasekaran, N., Mukherjee, A., 2020a. A review on tetracycline removal from aqueous systems by advanced treatment techniques. RSC Adv. 10, 27081–27095.

Gopal, G., Ravikumar, K., Salma, M., Chandrasekaran, N., Mukherjee, A., 2020b. Green synthesized Fe/Pd and in-situ Bentonite-Fe/Pd composite for efficient tetracycline removal. J. Environ. Chem. Eng. 8, 104126.

Guo, Y., Huang, W., Chen, B., Zhao, Y., Liu, D., Sun, Y., Gong, B., 2017. Removal of tetracycline from aqueous solution by MCM-41-zeolite A loaded nano zero valent iron: synthesis, characteristic, adsorption performance and mechanism. J. Hazard. Mater. 339, 22–32.

Hashemi, M., Amin, M.M., Sadeghi, S., Menglizadeh, N., Mohammadi, F., Patastar, S., Chavoshani, A., Rezaei, S., 2017. Coupling adsorption by NiO nanopowder with UV/H2O2 process for Cr (VI) removal. J. Adv. Environ. Health Res. 5, 210–219.

Hashemzadeh, F., Hasani, A., Ahmad Panahi, H., Borghei, S.M., 2018. Evaluation of the removal of heavy metals (cadmium lead, and zinc) from aqueous solutions using multi-walled carbon nanotubes modified with chitosan. J. Water Wastewater; Ab va Fazilab (in persian) 29, 31–41.

Jaafarzadeh, N., Ahmadi, M., Silva Martinez, S., Amiri, H., 2014. Removal of As (III) and As (V) from aqueous solution using modified solid waste vegetable oil industry as a natural adsorbent. Environ. Eng. Manage. J. (EEMJ) 13.

Jang, H.M., Yoo, S., Choi, Y.-K., Park, S., Kan, E., 2018. Adsorption isotherm, kinetic modeling and mechanism of tetracycline on Pinus taeda-derived activated biochar. Bioresour. Technol. 259, 24–31.

Javid, N., Nasiri, A., Malakootian, M., 2019. Removal of nonylphenol from aqueous solutions using carbonized date pits modified with ZnO nanoparticles. Desalin. Water Treat. 141, 140–148.

Jin, J., Yang, Z., Xiong, W., Zhou, Y., Xu, R., Zhang, Y., Cao, J., Li, X., Zhou, C., 2019. Cu and Co nanoparticles co-doped MIL-101 as a novel adsorbent for efficient removal of tetracycline from aqueous solutions. Sci. Total Environ. 650, 408–418.

Khan, A., Aziz, H., Khan, N., Hasan, M., Ahmed, S., Farooqi, I., Dhingra, A., Vambol, V., Changani, F., Yousefi, M., 2021. Impact, disease outbreak and the eco-hazards associated with pharmaceutical residues: a critical review. Int. J. Environ. Sci. Technol., 1–12

Khan, N.A., Ahmed, S., Farooqi, I.H., Ali, I., Vambol, V., Changani, F., Yousefi, M., Vambol, S., Khan, S.U., Khan, A.H., 2020. Occurrence, sources and conventional treatment techniques for various antibiotics present in hospital wastewaters: a critical review. TrAC, Trends Anal. Chem. 129, 115921.

Khoshnamvand, N., Jafari, A., Kamarehie, B., Faraji, M., 2019a. Optimization of adsorption and sonocatalytic degradation of fluoride by zeolitic imidazole framework-8 (ZIF-8) using RSM-CCD. Desalin Water Treat 171, 270–280.

Khoshnamvand, N., Jafari, A., Kamarehie, B., Mohammadi, A., Faraji, M., 2019b. Removal of malachite green dye from aqueous solutions using Zeolitic imidazole Framework-8. Environ. Processes 6, 757–772.

Kurian, M., Thankachan, S., 2021. Structural diversity and applications of spinel ferrite core-Shell nanostructures-a review. Open Ceramics 100179.

Li, J., Jiang, B., Liu, Y., Qiu, C., Hu, J., Qian, G., Guo, W., Ngo, H. H., 2017. Preparation and adsorption properties of magnetic chitosan composite adsorbent for Cu2 + removal. J. Cleaner Prod. 158, 51–58.

Liu, T., Liu, L., Gong, X., Chi, F., Ma, Z., 2021. Fabrication and comparison of active films from chitosan incorporating different spice extracts for shelf life extension of refrigerated pork. LWT 135, 110181.

Liu, Y., Li, J., Wu, L., Shi, Y., He, Q., Chen, J., Wan, D., 2020. Magnetic spent bleaching earth carbon (Mag-SBE@ C) for efficient adsorption of tetracycline hydrochloride: Response surface methodology for optimization and mechanism of action. Sci. Total Environ. 722, 137817.

Lu, H., Li, Y., Wang, Y., Li, X., 2019. Preparation of CoFe2O4@ vacancy@ mSiO2 core-shell composites for removal of organic pollutant in aqueous solution. J. Saudi Chem. Soc. 23, 536–545.

Mahdizadeh, H., Nasiri, A., Gharaghani, M.A., Yazdanpanah, G., 2020. Hybrid UV/COP advanced oxidation process using ZnO as a catalyst immobilized on a stone surface for degradation of acid red 18 dye. MethodsX 7.

Malakootian, M., Hashemi, M., Toolabi, A., Nasiri, A., 2018a. Investigation of nickel removal using poly(amidoamine) generation 4 dendrimer (PAMAM G4) from aqueous solutions. J. Eng. Res. 6, 13–23.

Malakootian, M., Kannan, K., Gharaghani, M.A., Dehdarirad, A., Nasiri, A., Shahamat, Y.D., Mahdizadeh, H., 2019a. Removal of metronidazole from wastewater by Fe/charcoal micro electrolysis fluidized bed reactor. J. Environ. Chem. Eng. 7.

Malakootian, M., Mahdizadeh, H., Khavari, M., Nasiri, A., Gharaghani, M.A., Khatami, M., Sahle-Demessie, E., Varma, R. S., 2020a. Efficiency of novel Fe/charcoal/ultrasonic micro-electrolysis strategy in the removal of Acid Red 18 from aqueous solutions. J. Environ. Chem. Eng. 8.

Malakootian, M., Nasiri, A., Alibeigi, A.N., Mahdizadeh, H., Gharaghani, M.A., 2019b. Synthesis and stabilization of ZnO nanoparticles on a glass plate to study the removal efficiency of acid red 18 by hybrid advanced oxidation process (Ultraviolet/ZnO/ultrasonic). Desalin. Water Treat. 170, 325–336.

Malakootian, M., Nasiri, A., Asadipour, A., Kargar, E., 2019c. Facile and green synthesis of ZnFe2O4@CMC as a new magnetic nanophotocatalyst for ciprofloxacin degradation from aqueous media. Process Saf. Environ. Prot. 129, 138–151.

Malakootian, M., Nasiri, A., Heidari, M.R., 2020b. Removal of phenol from steel plant wastewater in three dimensional electrochemical (TDE) process using CoFe2O4@AC/H2O2. Z. Phys. Chem. 234, 1661–1679.

Malakootian, M., Nasiri, A., Khatami, M., Mahdizadeh, H., Karimi, P., Ahmadian, M., Asadzadeh, N., Heidari, M.R., 2019d. Experimental data on the removal of phenol by electro-H2O2 in presence of UV with response surface methodology. MethodsX 6, 1188–1193.

Malakootian, M., Nasiri, A., Mahdizadeh, H., 2018b. Preparation of CoFe2O4/activated carbon@ chitosan as a new magnetic nanobiocomposite for adsorption of ciprofloxacin in aqueous solutions. Water Sci. Technol. 78, 2158–2170.

Malakootian, M., Nasiri, A., Mahdizadeh, H., 2019e. Metronidazole adsorption on CoFe2O4 /activated carbon@chitosan as a new magnetic biocomposite: Modelling, analysis, and optimization by response surface methodology. Desalin. Water Treat. 164, 215–227.

Malakootian, M., Nasiri, A., Mahdizadeh, H., 2019f. Metronidazole adsorption on CoFe2O4/Activated Carbon@ Chitosan as a new magnetic biocomposite: modelling, analysis, and optimization by response surface methodology. Desalin. Water Treat. 164, 215–227.

Malakootian, M., Smith, A., Gharaghani, M.A., Mahdizadeh, H., Nasiri, A., Yazdanpanah, G., 2020c. Decoloration of textile Acid Red 18 dye by hybrid UV/COP advanced oxidation process using ZnO as a catalyst immobilized on a stone surface. Desalin. Water Treat. 182, 385–394.

Malakootian, M., Yaseri, M., Faraji, M., 2019g. Removal of antibiotics from aqueous solutions by nanoparticles: a systematic review and meta-analysis. Environ. Sci. Pollut. Res. 26, 8444–8458.

Malakootiana, M., Farajib, M., Malakootianb, M., Nozarib, M., 2021. Ciprofloxacin removal from aqueous media by adsorption process: a systematic review and meta-analysis. Desalin. Water Treat. 229, 252–282.

Maleky, S., Asadipour, A., Nasiri, A., Luque, R., Faraji, M., 2022. Tetracycline Adsorption from Aqueous Media by Magnetically Separable Fe3O4@ Methylcellulose/APTMS: Isotherm, Kinetic and Thermodynamic Studies. J. Polym. Environ., 1–17

Malhotra, M., Suresh, S., Garg, A., 2018. Tea waste derived activated carbon for the adsorption of sodium diclofenac from wastewater: adsorbent characteristics, adsorption isotherms, kinetics, and thermodynamics. Environ. Sci. Pollut. Res. 25, 32210–32220.

Mallapur, M., Shaikh, P., Kambale, R., Jamadar, H., Mahamuni, P., Chougule, B., 2009. Structural and electrical properties of nanocrystalline cobalt substituted nickel zinc ferrite. J. Alloy. Compd. 479, 797–802.

Mehdinejad, M.H., Mengelizadeh, N., Bay, A., Pourzamani, H., Hajizadeh, Y., Niknam, N., Moradi, A.H., Hashemi, M., Mohammadi, H., 2018. Adsorption of methylene blue from aqueous solutions by cellulose and nanofiber cellulose and its electrochemical regeneration. Desalin. Water Treat. 110, 250–263.

Meroufel, B., Benali, O., Benyahia, M., Benmoussa, Y., Zenasni, M., 2013. Adsorptive removal of anionic dye from aqueous solutions by Algerian kaolin: Characteristics, isotherm, kinetic and thermodynamic studies. J. Mater. Environ. Sci 4, 482–491.

Mittal, H., Ray, S.S., Okamoto, M., 2016. Recent Progress on the Design and Applications of Polysaccharide-Based Graft Copolymer Hydrogels as Adsorbents for Wastewater Purification. Macromol. Mater. Eng. 301, 496–522.

Mmelesi, O.K., Masunga, N., Kuvarega, A., Nkambule, T.T., Mamba, B.B., Kefeni, K.K., 2020. Cobalt ferrite nanoparticles and nanocomposites: Photocatalytic, antimicrobial activity and toxicity in water treatment. Mater. Sci. Semicond. Process., 105523

Moghaddam, M.H., Nabizadeh, R., Dehghani, M.H., Akbarpour, B., Azari, A., Yousefi, M., 2019. Performance investigation of Zeolitic Imidazolate framework–8 (ZIF-8) in the removal of trichloroethylene from aqueous solutions. Microchem. J. 150, 104185.

Mohammadi, F., Yavari, Z., Rahimi, S., Hashemi, M., 2019. Artificial neural network modeling of Cr (VI) biosorption from aqueous solutions. J. Water Chem. Technol. 41, 219–227.

Mohammed, A.A., Kareem, S.L., 2019. Adsorption of tetracycline fom wastewater by using Pistachio shell coated with ZnO nanoparticles: Equilibrium, kinetic and isotherm studies. Alexandria Eng. J. 58, 917–928.

Naddafi, K., Martinez, S.S., Nabizadeh, R., Yaghmaeian, K., Shahtaheri, S.J., Amiri, H., 2021. Chlorpyrifos remediation in agriculture runoff with homogeneous solar photo-Fenton reaction at near neutral pH: phytotoxicity assessment. Water Sci. Technol. 83, 212–222.

Naddafi, K., Nabizadeh, R., Silva-Martinez, S., Shahtaheri, S.J., Yaghmaeian, K., Badiei, A., Amiri, H., 2018. Modeling of chlorpyrifos degradation by TiO2 photo catalysis under visible light using response surface methodology. Desalin. Water Treat. 106, 220–225.

Nasiri, A., Malakootian, M., Heidari, M.R., Asadzadeh, S.N., 2021a. CoFe2O4@Methylcelloluse as a New Magnetic Nano Biocomposite for Sonocatalytic Degradation of Reactive Blue 19. J. Polym. Environ. 29, 2660–2675.

Nasiri, A., Malakootian, M., Shiri, M.A., Yazdanpanah, G., Nozari, M., 2021b. CoFe 2 O 4@ methylcellulose synthesized as a new magnetic nanocomposite to tetracycline adsorption: modeling, analysis, and optimization by response surface methodology. J. Polym. Res. 28, 1–23.

Nasiri, A., Rajabi, S., Hashemi, M., 2022. CoFe2O4@ Methylcellulose/AC as a New, Green, and Eco-friendly Nano-magnetic Adsorbent for Removal of Reactive Red 198 from Aqueous Solution. Arabian J. Chem. 103745.

Nasiri, A., Tamaddon, F., Mosslemin, M.H., Faraji, M., 2019. A microwave assisted method to synthesize nanoCoFe2O4@methyl cellulose as a novel metal-organic framework for antibiotic degradation. MethodsX 6, 1557–1563.
Nasseh, N., Barikbin, B., Taghavi, L., Nasseri, M.A., 2019. Adsorption of metronidazole antibiotic using a new magnetic nanocomposite from simulated wastewater (isotherm, kinetic and thermodynamic studies). Compos. B Eng. 159, 146–156.
Noori Shamsi, M.H., Jafari, M., Shahin, M., 2018. A Review on Natural Adsorbents/Nano-adsorbents Based on Chitosan for Removal of Metal Contaminants from Water. J. Water Wastewater Sci. Eng. 3, 44–60.
Ofomaja, A.E., Naidoo, E.B., Pholosi, A., 2020. Intraparticle diffusion of Cr (VI) through biomass and magnetite coated biomass: A comparative kinetic and diffusion study. S. Afr. J. Chem. Eng. 32, 39–55.
Okoli, C.P., Ofomaja, A.E., 2019. Development of sustainable magnetic polyurethane polymer nanocomposite for abatement of tetracycline antibiotics aqueous pollution: Response surface methodology and adsorption dynamics. J. Cleaner Prod. 217, 42–55.
Oliveira, R.L., Vieira, J.G., Barud, H.S., Assunção, R., R Filho, G., Ribeiro, S.J., Messadeqq, Y., 2015. Synthesis and characterization of methylcellulose produced from bacterial cellulose under heterogeneous condition. J. Braz. Chem. Soc. 26, 1861–1870.
Pellicer, J.A., Rodríguez-López, M.I., Fortea, M.I., Hernández, J.A. G., Lucas-Abellán, C., Mercader-Ros, M.T., Serrano-Martínez, A., Núñez-Delicado, E., Cosma, P., Fini, P., 2018. Removing of Direct Red 83: 1 using α-and HP-α-CDs polymerized with epichlorohydrin: Kinetic and equilibrium studies. Dyes Pigm. 149, 736–746.
Pourzamani, H., Hashemi, M., Bina, B., Rashidi, A., Amin, M.M., Parastar, S., 2018. Toluene removal from aqueous solutions using single-wall carbon nanotube and magnetic nanoparticle–hybrid adsorbent. J. Environ. Eng. 144, 04017104.
Pourzamani, H., Parastar, S., Hashemi, M., 2017. The elimination of xylene from aqueous solutions using single wall carbon nanotube and magnetic nanoparticle hybrid adsorbent. Process Saf. Environ. Prot. 109, 688–696.
Qiu, W., Yang, D., Xu, J., Hong, B., Jin, H., Jin, D., Peng, X., Li, J., Ge, H., Wang, X., 2016. Efficient removal of Cr (VI) by magnetically separable CoFe2O4/activated carbon composite. J. Alloys Comp. 678, 179–184.
RAEIATBINA, P., AÇıKELB, Y.S., 2017. Removal of tetracycline by magnetic chitosan nanoparticles from medical wastewaters. Desalin. Water Treat. 73, 380–388.
Rajabi, S., Nasiri, A., Hashemi, M., 2022. Enhanced activation of persulfate by CuCoFe2O4@ MC/AC as a novel nanomagnetic heterogeneous catalyst with ultrasonic for metronidazole degradation. Chemosphere 286, 131872.
Riahi, K., Chaabane, S., Thayer, B.B., 2017. A kinetic modeling study of phosphate adsorption onto Phoenix dactylifera L. date palm fibers in batch mode. J. Saudi Chem. Soc. 21, S143–S152.
Rodrigues Filho, G., De Assunção, R.M., Vieira, J.G., Meireles, C. D.S., Cerqueira, D.A., Da Silva Barud, H., Ribeiro, S.J., Messaddeq, Y., 2007. Characterization of methylcellulose produced from sugar cane bagasse cellulose: Crystallinity and thermal properties. Polym. Degrad. Stab. 92, 205–210.
Sadeghi, S., Raki, G., Amini, A., Mengelizadeh, N., Amin, M.M., Hashemi, M., 2018. Study of the effectiveness of the third generation polyamideamine and polypropylene imine dendrimers in removal of reactive blue 19 dye from aqueous solutions. Environ. Health Eng. Manage. J. 5, 197–203.
Santhosh, C., Daneshvar, E., Kollu, P., Peräniemi, S., Grace, A.N., Bhatnagar, A., 2017. Magnetic SiO2@ CoFe2O4 nanoparticles decorated on graphene oxide as efficient adsorbents for the removal of anionic pollutants from water. Chem. Eng. J. 322, 472–487.
Sekiguchi, Y., Sawatari, C., Kondo, T., 2003. A gelation mechanism depending on hydrogen bond formation in regioselectively substituted O-methylcelluloses. Carbohydr. Polym. 53, 145–153.
Seow, T.W., Lim, C.K., Nor, M.H.M., Mubarak, M., Lam, C.Y., Yahya, A., Ibrahim, Z., 2016. Review on wastewater treatment technologies. Int. J. Appl. Environ. Sci 11, 111–126.
Singh, J., Yadav, P., Pal, A.K., Mishra, V., 2020. Water pollutants: Origin and status. Sensors in Water Pollutants Monitoring: Role of Material. Springer.
Singh, M.R., Gupta, A. 2016. Water pollution-sources, effects and control. Centre for Biodiversity, Department of Botany, Nagaland University.
Soares, V., Moraes, A.F.D.S.D., Santos, J.D., Grando, M.C., Luz, C. D., Colpani, G.L., Silva, L.L., Fiori, M.A., Mello, J.M.M.D., 2019. Obtaining of Fe3O4@ C Core-Shell Nanoparticles as an Adsorbent of Tetracycline in Aqueous Solutions. Mater. Res. 22.
Song, Q., Fang, Y., Liu, Z., Li, L., Wang, Y., Liang, J., Huang, Y., Lin, J., Hu, L., Zhang, J., 2017. The performance of porous hexagonal BN in high adsorption capacity towards antibiotics pollutants from aqueous solution. Chem. Eng. J. 325, 71–79.
Soori, M.M., Ghahramani, E., Kazemian, H., Al-Musawi, T.J., Zarrabi, M., 2016. Intercalation of tetracycline in nano sheet layered double hydroxide: an insight into UV/VIS spectra analysis. J. Taiwan Inst. Chem. Eng. 63, 271–285.
Soufi, A., Hajjaoui, H., Elmoubarki, R., Abdennouri, M., Qourzal, S., Barka, N., 2021. Spinel ferrites nanoparticles: Synthesis methods and application in heterogeneous Fenton oxidation of organic pollutants–A review. Appl. Surface Sci. Adv. 6, 100145.
Sun, X., Chen, F., Wei, J., Zhang, F., Pang, S., 2016. Preparation of magnetic triethylene tetramine-graphene oxide ternary nanocomposite and application for Cr (VI) removal. J. Taiwan Inst. Chem. Eng. 66, 328–335.
Takdastan, A., Mahvi, A.H., Lima, E.C., Shirmardi, M., Babaei, A.A., Goudarzi, G., Neisi, A., Heidari Farsani, M., Vosoughi, M., 2016. Preparation, characterization, and application of activated carbon from low-cost material for the adsorption of tetracycline antibiotic from aqueous solutions. Water Sci. Technol. 74, 2349–2363.
Tamaddon, F., Mosslemin, M.H., Asadipour, A., Gharaghani, M.A., Nasiri, A., 2020. Microwave-assisted preparation of ZnFe2O4@ methyl cellulose as a new nano-biomagnetic photocatalyst for photodegradation of metronidazole. Int. J. Biol. Macromol. 154, 1036–1049.
Varma, R., Vasudevan, S., 2020. Extraction, Characterization, and Antimicrobial Activity of Chitosan from Horse Mussel Modiolus modiolus. ACS Omega 5, 20224–20230.
Vinosha, P.A., Manikandan, A., Preetha, A.C., Dinesh, A., Slimani, Y., Almessiere, M., Baykal, A., Xavier, B., Nirmala, G.F., 2021. Review on recent advances of synthesis, magnetic properties, and water treatment applications of cobalt ferrite nanoparticles and nanocomposites. J. Supercond. Novel Magn., 1–24
WALDRON, R., 1955. Infrared spectra of ferrites. Phys. Rev. 99, 1727.
Wang, J., Zhuang, S., 2017. Removal of various pollutants from water and wastewater by modified chitosan adsorbents. Crit. Rev. Environ. Sci. Technol. 47, 2331–2386.
WEBER, JR, MORRIS, J.C., 1963. Closure to "Kinetics of Adsorption on Carbon from Solution. J. Sanitary Inst. Eng. Div. 89, 53–55.
Wiercigroch, E., Szafraniec, E., Czamara, K., Pacia, M.Z., Majzner, K., Kochan, K., Kaczor, A., Baranska, M., Malek, K., 2017. Raman and infrared spectroscopy of carbohydrates: A review. Spectrochim. Acta Part A Mol. Biomol. Spectrosc. 185, 317–335.
Xiong, W., Zeng, G., Yang, Z., Zhou, Y., Zhang, C., Cheng, M., Liu, Y., Hu, L., Wan, J., Zhou, C., 2018. Adsorption of tetracycline antibiotics from aqueous solutions on nanocomposite multi-walled carbon nanotube functionalized MIL-53 (Fe) as new adsorbent. Sci. Total Environ. 627, 235–244.
Xu, J., Xin, P., Han, Y., Wang, P., Jin, H., Jin, D., Peng, X., Hong, B., Li, J., Ge, H., 2014. Magnetic response and adsorptive properties for methylene blue of CoFe2O4/CoxFey/activated carbon magnetic composites. J. Alloy. Compd. 617, 622–626.

Yaghmaeian, K., Silva Martinez, S., Hoseini, M., Amiri, H., 2016. Optimization of As (III) removal in hard water by electrocoagulation using central composite design with response surface methodology. Desalin. Water Treat. 57, 27827–27833.

Yousefi, M., Gholami, M., Oskoei, V., Mohammadi, A.A., Baziar, M., Esrafili, A., 2021. Comparison of LSSVM and RSM in simulating the removal of ciprofloxacin from aqueous solutions using magnetization of functionalized multi-walled carbon nanotubes: Process optimization using GA and RSM techniques. J. Environ. Chem. Eng. 9, 105677.

Zhang, J., Xie, Q., Wang, Y., Liu, J., Yao, X. The preparation and environmental applications of magnetic activated carbon. In: 2011 International Conference on Electrical and Control Engineering, 2011. IEEE, pp. 1831–1834.

Zhang, X., Lin, X., He, Y., Chen, Y., Luo, X., Shang, R., 2019. Study on adsorption of tetracycline by Cu-immobilized alginate adsorbent from water environment. Int. J. Biol. Macromol. 124, 418–428.

Zhang, Y., Yan, T., Yan, L., Guo, X., Cui, L., Wei, Q., Du, B., 2014. Preparation of novel cobalt ferrite/chitosan grafted with graphene composite as effective adsorbents for mercury ions. J. Mol. Liq. 198, 381–387.

Zhao, R., Ma, T., Zhao, S., Rong, H., Tian, Y., Zhu, G., 2020a. Uniform and stable immobilization of metal-organic frameworks into chitosan matrix for enhanced tetracycline removal from water. Chem. Eng. J. 382, 122893.

Zhao, Z., Zhang, G., Zhang, Y., Dou, M., Li, Y., 2020b. Fe3O4 accelerates tetracycline degradation during anaerobic digestion: Synergistic role of adsorption and microbial metabolism. Water Res. 185, 116225.

Zhou, J., Ma, F., Guo, H., 2020. Adsorption behavior of tetracycline from aqueous solution on ferroferric oxide nanoparticles assisted powdered activated carbon. Chem. Eng. J. 384, 123290.

Zhou, L., Ji, L., Ma, P.-C., Shao, Y., Zhang, H., Gao, W., Li, Y., 2014. Development of carbon nanotubes/CoFe2O4 magnetic hybrid material for removal of tetrabromobisphenol A and Pb (II). J. Hazard. Mater. 265, 104–114.

Ziegler-Borowska, M., Chełminiak, D., Kaczmarek, H., 2015. Thermal stability of magnetic nanoparticles coated by blends of modified chitosan and poly (quaternary ammonium) salt. J. Therm. Anal. Calorim. 119, 499–506.